

**THERMOTROPIC AND LYOTROPIC LIQUID CRYSTAL
BEHAVIOUR OF AMPHIPHILIC MANNOSIDES**

MELONNEY PATRICK

**FACULTY OF SCIENCE
UNIVERSITY OF MALAYA
KUALA LUMPUR**

2018

**THERMOTROPIC AND LYOTROPIC LIQUID CRYSTAL
BEHAVIOUR OF AMPHIPHILIC MANNOSIDES**

MELONNEY PATRICK

**DISSERTATION SUBMITTED IN FULFILMENT
OF THE REQUIREMENTS FOR THE DEGREE OF
MASTER OF SCIENCE**

**DEPARTMENT OF CHEMISTRY
FACULTY OF SCIENCE
UNIVERSITY OF MALAYA
KUALA LUMPUR**

2018

UNIVERSITY OF MALAYA
ORIGINAL LITERARY WORK DECLARATION

Name of Candidate: MELONNEY PATRICK

Matric No: SGR140035

Name of Degree: Master of Science

Title of Project Paper/Research Report/Dissertation/Thesis (“this Work”):

THERMOTROPIC AND LYOTROPIC LIQUID CRYSTAL BEHAVIOUR
OF AMPHIPHILIC MANNOSIDES

Field of Study: Material Science

I do solemnly and sincerely declare that:

- (1) I am the sole author/writer of this Work;
- (2) This Work is original;
- (3) Any use of any work in which copyright exists was done by way of fair dealing and for permitted purposes and any excerpt or extract from, or reference to or reproduction of any copyright work has been disclosed expressly and sufficiently and the title of the Work and its authorship have been acknowledged in this Work;
- (4) I do not have any actual knowledge nor do I ought reasonably to know that the making of this work constitutes an infringement of any copyright work;
- (5) I hereby assign all and every rights in the copyright to this Work to the University of Malaya (“UM”), who henceforth shall be owner of the copyright in this Work and that any reproduction or use in any form or by any means whatsoever is prohibited without the written consent of UM having been first had and obtained;
- (6) I am fully aware that if in the course of making this Work I have infringed any copyright whether intentionally or otherwise, I may be subject to legal action or any other action as may be determined by UM.

Candidate’s signature

Date:

Subscribed and solemnly declared before,

Witness’s signature

Date:

Name:

Designation:

THERMOTROPIC AND LYOTROPIC LIQUID CRYSTAL BEHAVIOUR OF AMPHIPHILIC MANNOSIDES

ABSTRACT

Glycolipid consists of sugar head group bonded to hydrocarbon chain through a glycosidic link. It plays important biological functions in nature, such as endo- and exocytosis, apoptosis, and molecular recognition at the cell surface specific to the cell type. Synthetic glycolipid which closely mimic natural glycolipids are highly in demand as membrane model systems and it can be synthesized either chemically or enzymatically. Herein, five series of branched chain glycolipids with mannose as the head group and different total chain length from C₈ to C₂₄ carbons have been prepared. The effect of chain branching on their liquid crystalline phases were investigated by optical polarizing microscopy (OPM), differential scanning calorimetry (DSC) and small-angle X-ray scattering (SAXS). A comparison of these showed that they have different mesomorphism as the chain length increases. In the dry state, the shorter chain compounds, α -Man-OC₆C₂ and α -Man-OC₈C₄ exhibit lamellar phase. The phase for middle chain mannoside, α -Man-OC₁₀C₆ could not be assigned conclusively at the room temperature, but this metastable phase transformed to lamellar above 37°C. Meanwhile, the longer chain compounds, α -Man-OC₁₂C₈ and α -Man-OC₁₄C₁₀ form inverse bicontinuous cubic phase of space group $Ia3d$ and inverse hexagonal phase, respectively. The lyotropic phase behaviour was determined using a contact penetration technique. In α -Man-OC₆C₂, the water rich side of the sample turned to an isotropic micellar solution. The α -Man-OC₈C₄ remains as lamellar phase upon hydration. An inverse bicontinuous cubic phase of space group $Pn3m$ is observed in the fully hydrated α -Man-OC₁₀C₆. Both α -Man-OC₁₂C₈ and α -Man-OC₁₄C₁₀ give inverse hexagonal phase in excess water. The

formation of lamellar and non-lamellar phases by these compounds makes them ideal candidates for a variety of applications such as controlled release drug-carrier.

Keywords: mannoside, glycolipids, thermotropic cubic phase

University of Malaya

SIFAT CECAIR HABLUR TERMOTROPIK DAN LIOTROPIK

AMFIFILIK MANNOSIDA

ABSTRAK

Glikolipid adalah molekul yang terdiri daripada kumpulan kepala gula yang terikat dengan rantaian hidrokarbon melalui pautan glikosida. Ia memainkan fungsi biologi yang penting dalam alam semulajadi, seperti endo- dan eksositosis, apoptosis, dan pengesanan molekul pada permukaan sel khusus kepada jenis sel. Analog yang hampir menyerupai glikolipid semulajadi sangat diperlukan sebagai model sistem membran dan boleh disintesis sama ada secara kimia atau enzimatik. Dalam projek ini, lima siri rantaian cabang glikolipid yang mempunyai mannosida sebagai kumpulan kepala dengan jumlah rantai alkil yang berbeza daripada karbon C₈ hingga C₂₄ telah disediakan. Kesan rantaian cabang pada fasa cecair hablur ini dikaji menggunakan mikroskopi optik berkutub (OPM), kalorimetrik pengimbas pembeza (DSC) dan serakan sinar-X bersudut-kecil (SAXS). Perbandingan ini menunjukkan bahawa mereka mempunyai mesofasa yang berbeza dengan peningkatan panjang rantai. Dalam keadaan kering, sebatian rantai yang lebih pendek, α -Man-OC₆C₂ dan α -Man-OC₈C₄ menunjukkan fasa lamelar. Rantaian tengah mannosida, α -Man-OC₁₀C₆ tidak menunjukkan fasa yang jelas pada suhu bilik. Namun, fasa metastabil ini membentuk fasa lamelar pada suhu melebihi 37°C. Sementara itu, sebatian rantai yang lebih panjang, iaitu α -Man-OC₁₂C₈ dan α -Man-OC₁₄C₁₀ masing-masing membentuk fasa kubus dwiselanjar terbalik dengan kumpulan simetri *Ia3d* dan fasa heksagonal terbalik. Tingkah laku fasa liotropik ditentukan melalui kaedah penembusan air. Bagi α -Man-OC₆C₂, kawasan tinggi kandungan air bertukar kepada fasa isotropik yang merujuk kepada larutan miselar. α -Man-OC₈C₄ kekal sebagai fasa lamelar semasa penghidratan. Fasa kubus dwiselanjar terbalik dengan kumpulan simetri *Pn3m* dapat dilihat pada α -Man-OC₁₀C₆ yang terhidrat sepenuhnya. Kedua-dua α -Man-OC₁₂C₈ dan α -Man-OC₁₄C₁₀ memberikan fasa heksagonal terbalik dalam air berlebihan.

Pembentukan fasa lamelar dan bukan lamelar pada sebatian ini menjadikannya ideal untuk pelbagai aplikasi seperti kawalan pelepasan ubat.

Kata kunci: mannosida, glikolipid, fasa kubik termotropik

University of Malaya

ACKNOWLEDGEMENTS

I would like to express my sincere gratitude to my advisor Dr. Noor Idayu Mat Zahid for the continuous support of my master study and research, for her patience, motivation, enthusiasm, and immense knowledge. Her guidance helped me in all the time of research and writing of this thesis. I could not have imagined having a better advisor and mentor for my master study.

The door to Professor Dr. Rauzah Hashim office was always open whenever I ran into a trouble spot or had a question about my research or writing and for her insightful comments and encouragement, but also for the hard question which incited me to widen my research from various perspectives.

Getting through my dissertation required more than academic support, and I have many, many people to thank for listening to and, at times, having to tolerate me over the past three years. I cannot begin to express my gratitude and appreciation for their friendship. I must thank everyone above as well as Dr. Malinda Salim, Dr. Matiur Rahman, Liew Chia Yen, Nur Asmak Nabila and Wan Farah Nasuha for their unwavering in their personal and professional support during the time I spent at this University.

Most importantly, none of this could have happened without my family. I must express my very profound gratitude to my parents and to my friends for providing me with unfailing support and continuous encouragement throughout my years of study and through the process of researching and writing this thesis. This accomplishment would not have been possible without them. Thank you.

TABLE OF CONTENT

Abstract	iii
Abstrak	v
Acknowledgement	vii
Table of Contents	viii
List of Figures	xi
List Tables	xiv
List of Schemes	xv
List of Symbols and Abbreviations	xvi
List of Appendices	xviii
CHAPTER 1: INTRODUCTION	1
1.1 Thermotropic Liquid Crystal	3
1.1.1 Nematic	4
1.1.2 Smectic	5
1.2 Lyotropic Liquid Crystal	7
1.2.1 Micelle	7
1.2.2 Lamellar (L_{α})	8
1.2.3 Hexagonal	9
1.2.4 Cubic (I, V)	10
1.3 Order Parameter	12
1.4 Curvature Forces in Lipid Interaction	13

CHAPTER 2: LITERATURE REVIEW	15
2.1 Natural Glycolipid	15
2.1.1 Guerbet Glycolipids	16
2.1.2 Mannose Base Glycolipids	17
2.2 Objectives of Study	19
CHAPTER 3: METHODOLOGY	20
3.1 Synthesis of Guerbet Mannosides	20
3.1.1 Materials	23
3.1.2 Characterization using Nuclear Magnetic Resonance (NMR)	24
3.1.3 General Peracetylation Procedure: Synthesis of α -mannose pentacetate	24
3.1.4 General Glycosidation Procedure: Synthesis of α -alkyl mannosides	25
3.1.5 General Deacetylation Procedure	25
3.2 Liquid Crystal Phase Behaviour	26
3.2.1 Fourier transform infrared spectroscopy (FTIR)	26
3.2.2 Differential Scanning Calorimetry (DSC)	27
3.2.3 Optical Polarizing Microscopy (OPM)	28
3.2.4 Small Angle X-ray Scattering (SAXS)	33
CHAPTER 4: RESULTS AND DISCUSSION	37
4.1 Synthesis of the Guerbet Mannosides	38
4.2 Liquid Crystal Phase Behaviours of Guerbet Mannosides	41
4.2.1 Thermotropic Phase Behaviour	41
4.2.2 Lyotropic Phase Behaviour	53

CHAPTER 5: CONCLUSION	59
References	62
List of Publications and Papers Presented	71
Appendix	74

University of Malaya

LIST OF FIGURES

Figure 1.1	Relationship of liquid crystalline phase with liquid and crystalline solid (An et al., 2016) (Redrawn).	2
Figure 1.2	Spherical micelle structures: (a) normal (L_1) and (b) inverse (L_2) (Redrawn).	8
Figure 1.3	Lamellar lyotropic liquid crystal: (a) molecular arrangement (b) possible optical textures (c) example of lamellar LLC (sodium cholate) (Redrawn).	9
Figure 1.4	Comparison of (a) normal (H_1) and (b) inverse (H_2) hexagonal phases (Seddon, 1990) (Redrawn).	10
Figure 1.5	Sketch of bicontinuous cubic phase namely (a) $Ia3d$, b) $Pn3m$ and c) $Im3m$ (Redrawn).	11
Figure 1.6	Structures of discontinuous cubic namely, (a) body-centered cubic and (b) face-centered cubic (Redrawn).	11
Figure 1.7	The schematic diagram of a nematic phase where molecules are distributed about the local director $\uparrow \mathbf{n}$, θ is the angle between the molecular long axis and the director (Redrawn).	12
Figure 2.1	Natural glycolipid: (a) typical structure and some examples: (b) monogalactosyl-diacylglycerol (MGDG) (c) digalactosyldiacylglycerol (DGDG) (d) ceramide (e) β -hexosaminidase (Redrawn).	15
Figure 2.2	Chemical structures of D-mannose (a) comparing mannose with glucose and fructose (b) polymer of mannose (Hu et al., 2016) (Redrawn).	18
Figure 3.1	Different hydroxyl (-OH) group of mannose and glucose at C2 position	20
Figure 3.2	Principle of heat flux (Auroux, 2013)	27
Figure 3.3	Components parts of optical polarizing microscope (Murphy, 2002)	29
Figure 3.4	An image that magnified in the microscope (Redrawn)	30
Figure 3.5	Basic principle of optical polarizing microscope (“Microscope Primer”, 2017)	30
Figure 3.6	Preparation of sample onto the glass microscope (Redrawn)	31

Figure 3.7	Contact preparation used for the study of lyotropic behaviour (Redrawn)	32
Figure 3.8	Mettler Toledo FP90 central processor (“Mettler Toledo”, 2017)	32
Figure 3.9	Mettler Toledo FP82HT hot stage (“Thermal Microscopy Hot Stage”, 2017)	33
Figure 3.10	The setup of X-ray scattering experiment (“Dimensional Metrology for Nanofabrication”, 2009) (Redrawn).	34
Figure 3.11	Bragg expressed for SAXS at 7° (Werneck et al., 2013)	34
Figure 3.12	Bragg expressed for WAXS at 45° (Werneck et al., 2013)	35
Figure 4.1	The chemical structures of the Guerbet branched α -D-mannosides	37
Figure 4.2	FTIR spectra for α -Man-OC ₁₄ C ₁₀ at the room temperature in dry (after lyophilized in freeze dryer for at least 48 hours), left in ambient moisture for 96 hours and in excess water form and (b) FTIR spectra for water at room temperature	42
Figure 4.3	DSC thermograms for dry α -D-mannosides at a heating scanning rate of 5°C min ⁻¹	43
Figure 4.4	Textures of dry α -D-mannosides at 25°C, viewed under an optical polarizing microscope with x10 magnification: (a-c) show textures of L _{α} phase observed for α -Man-OC ₆ C ₂ , α -Man-OC ₈ C ₄ and α -Man-OC ₁₀ C ₆ respectively; (d) a cubic phase V ₂ is observed for α -Man-OC ₁₂ C ₈ ; (e) an inverse hexagonal (H ₂) for α -Man-OC ₁₄ C ₁₀	47
Figure 4.5	Small angle X-ray scattering patterns from dry Guerbet branched α -D-mannosides at 25°C. Patterns are offset along the y-axis for clarity. (a) L _{α} ; (b) the two different size L _{α} phases and * unassigned peak; (c) a metastable phase; (d) an inverse bicontinuous cubic phase with space group <i>Ia3d</i> phase and (e) H ₂ phase	51
Figure 4.6	SAXS pattern as a function of temperature for (a) α -Man-OC ₆ C ₂ , (b) α -Man-OC ₈ C ₄ , (c) α -Man-OC ₁₀ C ₆ , (d) α -Man-OC ₁₂ C ₈ and (e) α -Man-OC ₁₄ C ₁₀	52
Figure 4.7	WAXS pattern at 25°C for (a) α -Man-OC ₈ C ₄ and (b) α -Man-OC ₁₀ C ₆	53

- Figure 4.8** Contact penetration textures of Guerbet branched α -D-mannosides, viewed under an optical polarizing microscope ($\times 10$) at 30°C after 60 min: (a) normal micellar, L_1 ; (b) lamellar, L_{α} ; (c) inverse cubic, V_2 ; (d) inverse hexagonal, H_2 and (e) inverse hexagonal, H_2 55
- Figure 4.9** SAXS patterns for Guerbet branched-chain mannoside in excess water at 25°C . (a) L_1 micellar solution; (b) lamellar, L_{α} ; (c) inverse bicontinuous cubic ($Pn3m$) and asterisk, * indicates an extra peak of another phase present at 25°C and the peak merged into a $Pn3m$ at 37°C . (d) inverse hexagonal, H_2 and (e) inverse hexagonal, H_2 56

University of Malaya

LIST OF TABLES

Table 1.1	Different arrangements of thermotropic liquid crystal phases (a) nematic, (b) discotic, (c) Smectic A, (d) Smectic C and (e) cholesteric with some examples and their corresponding textures	6
Table 4.1	Thermotropic phase transition temperatures T_m (melting) and T_c (clearing) for the dry α -D-mannosides determined by DSC and OPM. Asterisk (*) indicates the value is determined by OPM. ΔH_m and ΔH_c are enthalpies associated with melting and clearing transitions respectively. Errors in the measured transition temperature $\pm 1^\circ\text{C}$, while error in the enthalpy change is $\pm 0.1 \text{ kJ mol}^{-1}$. The symbol “-” denotes unknown value due to the limitation of the calorimeter. Phase identification is by OPM, except for the glassy phase, which is identified as lamellar glass ($L_{\alpha G}$). For comparison monoalkylated mannosides and other Guerbet α -glycosides (glucose, galactose and xylose) are included	44
Table 4.2	Small angle X-ray scattering data of the dry α -D-mannosides at 25°C . Error in lattice parameter measurements is $\pm 0.1 \text{ \AA}$. * indicates measurements taken at 37°C	53
Table 4.3	Small angle X-ray scattering data of the fully hydrated α -D-mannosides at 25°C . Error in lattice parameter is $\pm 0.1 \text{ \AA}$	57

LIST OF SCHEMES

Scheme 3.1	Overview of general glycosylation methods (Johansson, 2015)	21
Scheme 3.2	Reaction scheme to synthesize Guerbet mannose glycolipids series	22

University of Malaya

LIST OF SYMBOLS AND ABBREVIATIONS

% (w/w)	:	Mass fraction
σ	:	Electrical conductivity
λ	:	Wavelength
θ	:	Angle
ε	:	Dielectric constant
μ	:	Permeability
Δn	:	Birefringent
ΔH	:	Enthalpy
α	:	Alpha
Cr	:	Crystalline
CMC	:	Critical micelle concentration
DSC	:	Differential scanning calorimetry
e.g	:	for example
etc	:	Other things
FTIR	:	Fourier Transform Infrared Spectroscopy
Gal	:	Galactose
Glu	:	Glucose
H ₁	:	Normal hexagonal phase
H ₂	:	Inverse hexagonal phase
I	:	Discontinuous cubic phase
<i>Ia3d</i>	:	Gyroid lattice cubic phase
<i>Im3m</i>	:	Primitive lattice cubic phase
LC	:	Liquid Crystal
LLC	:	Lyotropic liquid crystal
L _{α}	:	Lamellar liquid crystal phase

L_1	:	Normal micellar phase
L_2	:	Inverse micellar phase
Man	:	Mannose
η	:	Viscosity
n	:	Director
NMR	:	Nuclear Magnetic Resonance
-OH	:	Hydroxyl group
OPM	:	Optical polarizing microscopy
$Pn3m$:	Double diamond lattice cubic phase
SAXS	:	Small angle X-ray scattering
SmA	:	Smectic A
SmC	:	Smectic C
T_m	:	Melting temperature
T_c	:	Clearing temperature
TLC	:	Thin layer chromatography
TPMS	:	Triply periodic minimal surface
V	:	Bicontinuous cubic phase
WAXS	:	Wide angle X-ray scattering

LIST OF APPENDICES

APPENDIX A	: ^1H - NMR SPECTRA	74
APPENDIX B	: ^{13}C -NMR SPECTRA	85
APPENDIX C	: DSC THERMOGRAMS	90
APPENDIX D	: FTIR SPECTRA	93

University of Malaya

CHAPTER 1: INTRODUCTION

The historical backdrop of liquid crystal (LC) begins with the discovery of liquids which give birefringent property due to the presence of defects which do not break the continuous liquid character of the phase, changing size, shape and depend on the static and dynamic boundary conditions (Kleman & Lavrentovich, 2009). These are also known as mesophases which possess an intermediate order structure. A mesophase is bounded by a phase transition at lower temperature from the crystalline solid which have a long range order and another transition at higher temperature into the amorphous liquid (isotropic) that does not have a particular order. It may be useful to recall some basic properties of liquid and crystal to understand more about liquid crystal. In a liquid phase, the centers of mass are not ordered. While in a crystal, the centers mass of the various groups are located on a three dimensional periodic lattice and regularly stacked. These two states of matter differ most obviously by their mechanical properties where a liquid flows easily and a solid does not (Prost, 1995).

LC is versatile, adaptable and exceedingly responsive because of the symmetry and its mechanical properties are intermediate to those of a liquid and a solid crystal. When it is exposed to an external perturbation such as an electric field, changing in temperature, pressure, pH, hydration and concentrations of inorganic ions, it undergoes a change in the orientation which eventually lead to a phase transition (Ho et al., 1996). Due to these features, the arrangement orientational and positional orders of the molecules within LC phases differ by their arrangements and consequently their physical properties. A liquid crystal phase contains long range orientational and positional orders either in zero, one, two or three dimensions. Hence, a LC shows mechanical stability like solid and flows like a liquid (An et al., 2016; Stevenson et al., 2005). Wunderlich defined broadly different states of matter which include gas, liquid, crystal and glass phases. The different states of

matter is related to molecular motions namely, translation, rotation and vibration (Stevenson et al., 2005). The phases of matter include solid, liquid and the intermediate liquid crystal phase as in Figure 1.1.

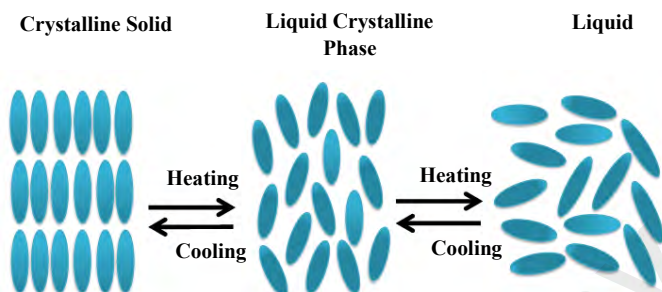


Figure 1.1: Relationship of liquid crystalline phase with liquid and crystalline solid (An et al., 2016) (Redrawn).

In 19th century, LC was discovered by Friedrich Reinitzer, an Austrian Botanist that found out of the unusual melting that was always accompanied by the presence of a cloudy state before a clear liquid appeared. He observed organic crystal of cholesteryl benzoate melted at the temperature of 145°C to become a cloudy state and then became clear at 179°C. This is the double melting behavior, which was a strange phenomenon. The sample was then sent to Otto Lehmann. He examined it under the microscope, which showed a birefringence and rainbow-like colors that raise a question about the phase transitions and the molecules that involved during the transition (Jenkins, 1978; Kelker, 1988). Reinitzer sent other samples in order to investigate the phenomenon. In the following years, this phenomenon was referred to as a flowing crystal by Lehmann and consequently the term of crystalline liquid was used in 1890 (Kelker, 1973).

Although the discovery of LC was observed since 1888, it took another 100 years before the applications of LC materials being acknowledged due to the important role in industry, biology and their potential for the applications in food , agriculture, medicine,

etc. (Rizvi, 2003). However, within this period interest in fundamental aspects of LCs continue (Parshin et al., 2013).

Two main classes of LCs are thermotropic and lyotropic LCs. A thermotropic LC determines the phase by changing the temperature. For example, the material is heated from usually the crystal state in the beginning until it melts into a liquid crystal phase at melting temperature (T_m) and continues being heated until reaching the clearing temperature (T_c) which is the transition into the isotropic liquid phase. On the other hand, a lyotropic LC requires an addition of solvent like water and to form a liquid crystal phase in which molecules organize into different structures including the isotropic phase called the micellar phase (Lagerwall & Scalia, 2012). Lyotropic LCs possess some essential features as thermotropic LCs, for example the nature of ordering within the phase. However, these liquid crystals vary broadly in structure, properties and applications (Stevenson et al., 2005).

1.1 Thermotropic Liquid Crystals

Small molar mass thermotropic LC compounds contain mostly of molecules which are either rod-shaped or disc-shaped (Gray, 1987). It can be additionally divided into various phases depending upon the degree of ordering in orientation and position (Jin et al., 1980). In general LC is birefringent, which means the optical property of LC material has a refractive index that depends on the polarization and propagation direction of light. LC material is optically anisotropic. The birefringence (Δn) is often quantified as the maximum difference between refractive indices along the parallel (n_o) and perpendicular (n_e) directions exhibited by the material, or $\Delta n = n_o - n_e$. Likewise, other properties such as dielectric constant (ϵ), permeability (μ), electrical conductivity (σ) and viscosity (η) measured in the direction of the long molecular axis are different from those measured in

the plane parallel to the long axis (Kawamoto, 2002). Georges Friedel proposed classification of the thermotropic LC into three main types, namely nematic, smectic and cholesteric. We shall discuss nematic and smectic liquid crystals in the following sections. Cholesteric LC is a form of nematic that contains a chiral center which makes the director (\mathbf{n}) twists in a helical fashion, which make it exhibit an interesting phenomena such as the optical rotation (Gray, 1987; Kawamoto, 2002; Wu, 1994). Table 1.1 shows different arrangements of thermotropic liquid crystal phases.

1.1.1 Nematic

Nematic liquid crystal was first used by Georges Friedel in his *Mesomorphic States of Matter* to the *Annales des Physiques* in 1922. It refers to a certain thread like defects that are commonly observed under the polarized microscope. The term comes from the Greek word “*nema*” which means thread-like. This phase has one-dimension long range orientational order and it possesses a simple director (\mathbf{n}) in one direction without positional order. The arrangement of the molecules in the nematic mesophase was made up of rod-like molecules and disc-like molecules (Prost, 1995). These rod- or disc-like molecules have a high symmetry usually assumed to be $D_{\infty h}$ and their symmetry axes remain parallel to each other. Thus the molecules and phase is assumed to be uniaxial (Dierking, 2003; Gray, 1987; Jenkins, 1978). Much investigation had been done not only for the biological systems but can apply for the development of the electric device performed by using the liquid crystal displays. Nematic liquid crystal possesses a better dielectric anisotropy and optical birefringence. A compound of 4-n-pentyl-4-cyanobiphenyl (5CB) is one of the typical core parts of LC compounds exhibiting nematic phases (Table 1.1) (Matsushita & Koseki, 2005). Optical polarizing microscopy have been commonly used to identify the nematic textures (Qi & Hegmann, 2006). Due to the microstructure of the nematic phase, it exhibits a birefringence because of the polarized

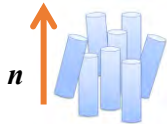
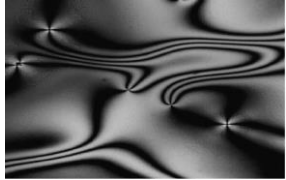

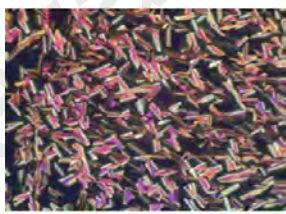
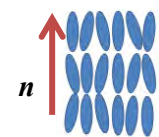


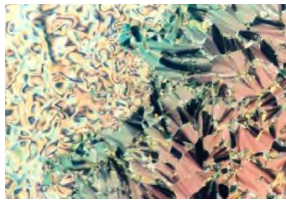
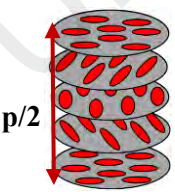
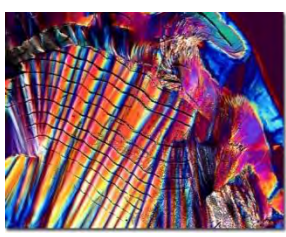
light since the refractive index in a direction along with long axis of molecules is different with the refractive index in the orthogonal direction.

1.1.2 Smectic

The smectic liquid crystal on the other hand is derived from the Greek word “smecticus”, meaning cleaning, or having soap-like properties. Thus, this phase has a soapy feeling when touch. It has a long range orientation order and positional order, characterized by smectic layers which are free to slip and move over each other and at the same time it is viscous (Chung, 1986; Vertogen & Wilhelmus, 2012). There are many different smectic phases which differ from one another in the degree of positional and orientational orders.

Smectic A phases have layered superstructures. The molecular long axes are on average parallel to the layer normal and the molecules have no directional order in their lateral directions (Kishikawa et al., 2011). The director is perpendicular to the smectic layer plane and the orientation order is long way from being perfect with a layer thickness that is about equal to the length of the molecule (Dierking, 2003; Vertogen & Wilhelmus, 2012). In smectic C, it looks similar to a smectic A but its director tilts by an angle with the normal layer and has one dimension position order. This lead to large separations of smectic planes due to the direction (Chen & Lubensky, 1976; Dierking, 2003).

Table 1.1: Different arrangements of thermotropic liquid crystal phases (a) nematic, (b) discotic, (c) Smectic A, (d) Smectic C and (e) cholesteric with some examples and their corresponding textures.

Phase	Typical Molecule	Texture
a) Nematic 	4-n-pentyl-4-cyanobiphenyl (5CB) Cr 22.4 N 34.5 Iso <chem>CCCCc1ccc(cc1)-c2ccc(cc2)C#N</chem>	
b) Discotic 	2,3,6,7,10,11-hexahexyloxytriphenylene Cr 70 Col _h 100 Iso <chem>CCCCCOc1ccc2c(c1)c3ccc(OC)cc3c2OC</chem>	
c) Smectic A 	4-n-octyl-4-cyano-biphenyl (8CB) C 21.5 SmA 33.5 N 40.5 Iso <chem>CCCCCCCc1ccc(cc1)-c2ccc(cc2)C#N</chem>	
d) Smectic C 	4-n-pentybenzenethio-4'-n decyl oxybenzoate C 60 SmC 63 SmA 80 N 86 Iso <chem>CCCCCOC(=O)c1ccc(cc1)Sc2ccc(cc2)C#N</chem>	
e) Cholesteric 	Cholesteryl benzoate CR 145 Cholesteric 178 Iso <chem>CC(C)CCCC[C@H]1CC[C@@H]2[C@@]1(CC[C@H]3[C@H]2CC=C4[C@@]3(CC[C@@H](C4)O)C)C</chem>	

1.2 Lyotropic Liquid Crystals

Lyotropic liquid crystals (LLC) can also be called lyomesophases. It occurs in the presence of solvents (usually water) at a given temperature. This mesophase is commonly found in the self-assembly of biological systems as well as in cosmetics and detergents (Neto & Salinas, 2005). Typically a lyotropic material comprises of molecules, each has a hydrophilic and hydrophobic parts. The addition of a solvent such as water will selectively hydrate the hydrophilic moiety of each molecule. In addition polar solvent like water will avoid the hydrophobic regions (Hyde, 2001). The concepts of hydrophilic (loves water) and hydrophobic (hates water) refers to the affinity of a particular molecule with a respect to the water molecules (Neto & Salinas, 2005). The interaction between the molecular units in the solution will form a well characterized phases like lamellar and hexagonal (Forrest & Reeves, 1981). In addition, lyotropic liquid crystals can also give rise to the cubic phases which are not observed frequently (Collings, 2002). Lyotropic phases have many applications for example they are potentially useful for drug vehicles (Forrest & Reeves, 1981; Gu et al., 2010).

1.2.1 Micelle

Micelle is a colloidal dispersions of self-assembled amphiphilic molecules where it has two affinity regions towards solvent, namely hydrophilic and hydrophobic. The hydrophilic regions are in-contact with the surrounding polar solvent and while the hydrophobic avoid solvent and self-arrange inside the micelle as a core. The opposite effect can be observed in the case of non-polar solvent (Figure 1.2) (Tanbour et al., 2016).

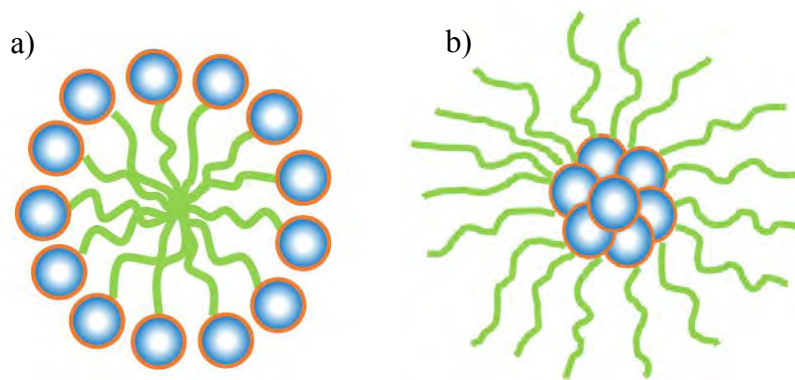


Figure 1.2: Spherical micelle structures: (a) normal (L_1) and (b) inverse (L_2) (Redrawn).

Micelle is formed when the solution is dilute and above the critical micelle concentration (CMC). Micelle is stable in water and the micellar solution behave as an isotropic fluid (Collings & Hird, 1997). Many preparation methods have been developed to make the micellar phase and usually a micelle forms in different size and shapes which require further stabilization technique (Maibaum et al., 2004; Rager et al., 1999). It is also important to understand on how the molecular structures of surfactants in a mixture affect the solution properties of the micelles, such as the CMC and the size and shape of the micelles. By this way, it helps in choosing a surfactant structures which will result in the desired performance properties (Shiloach & Blankschtein, 1998).

1.2.2 Lamellar (L_a)

The lamellar (L_a) lyotropic liquid crystal is illustrated in Figure 1.3 and as can be seen this particular phase consists of a layered arrangement of amphiphilic molecules. It is also called the neat soap phase where the layers are controlled by varying the amphiphilic water ratio (Dellinger & Braun, 2004; Lauger et al., 1995).

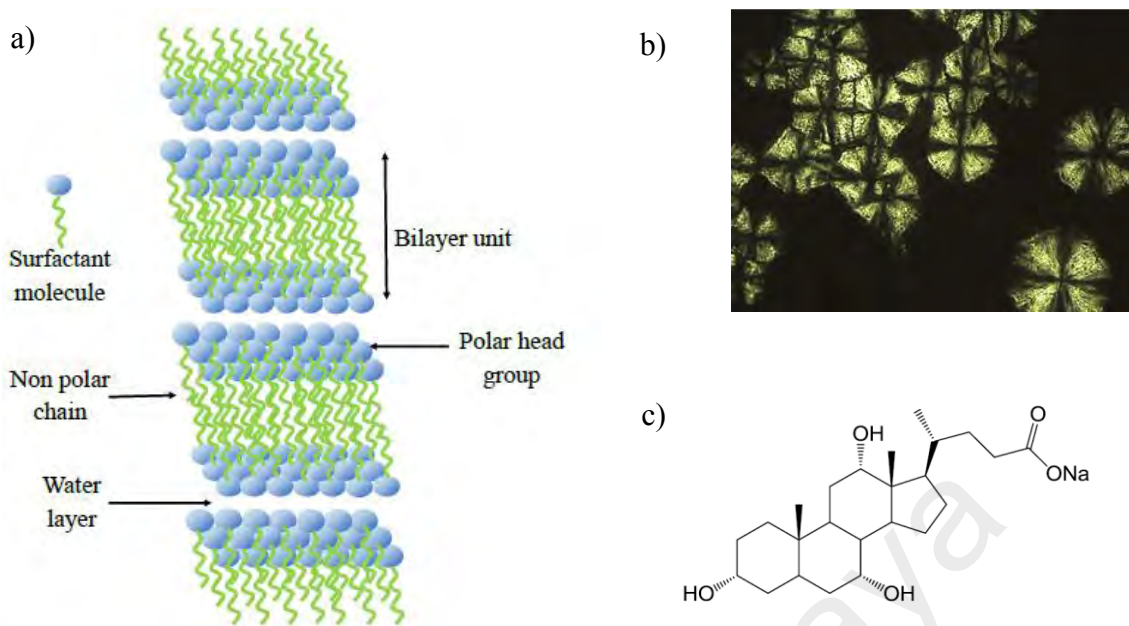


Figure 1.3: Lamellar lyotropic liquid crystal: (a) molecular arrangement (b) possible optical textures (c) example of lamellar LLC (sodium cholate) (Redrawn).

Meanwhile, in lamellar lyotropic liquid crystal, polar headgroups are aligned together at the interface of water and the non-polar chain are aligned parallel to one another 'hiding away' from water (see Figure 1.3). Lamellar phases have a long-range orientational order and one-dimensional long-range positional order. Similar to other anisotropic phases, it exhibits distinct optical textures when viewed under optical microscope. Typically, the textures are usually streaky or mosaic like (Hyde, 2001).

1.2.3 Hexagonal (H)

Adding more water leads to the formation of a hexagonal structure or also called as the middle soap phase which form long cylindrical rods arranged in parallel to a hexagonal array (Collings, 2002). These structures have molecular aggregate ordering which corresponds to a hexagonal arrangement (see Figure 1.4). There are two types of hexagonal phase, namely the normal hexagonal (H_1) and inverse hexagonal (H_2). H_1 phase is radially arranged in rods of indefinite length packed hexagonally in water and with non-polar hydrophobic tails directed inward. In H_2 phase, the hydrophilic parts point inward

into the water channel while the hydrophobic tails are directed outward (Deamer et al., 1970; Seddon, 1990). These hexagonal phases may be stable in excess water and these can be dispersed in water to form nanoparticles which can be useful for a biological system and controlled release of drug delivery. The hexagonal phase has the ability to provide slow drug release apart from protecting peptides, protein and nucleic acids from both chemical and physical degradation (Chen et al., 2014; Nguan et al., 2014).

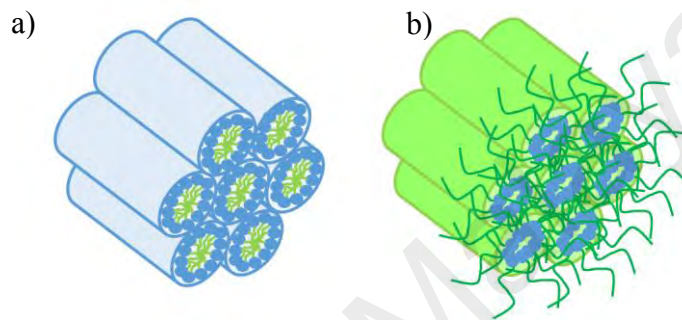


Figure 1.4: Comparison of (a) normal (H_1) and (b) inverse (H_2) hexagonal phases (Seddon, 1990) (Redrawn).

1.2.4 Cubic (I, V)

The lyotropic cubic phase is usually viscous and isotropic in nature and there are two types, the discontinuous (I) and the bicontinuous (V) ones. Bicontinuous (V) cubic phases consist of a single continuous curved lipid bilayer forming a complex network with 3-D cubic symmetry, which separates two continuous but non-intersecting water channels. Three types of bicontinuous cubic phases commonly found in nature are the gyroid lattice cubic phase ($Ia3d$) and the double diamond lattice cubic phase ($Pn3m$) and primitive lattice cubic phase ($Im3m$). These have low energy structures and can be influenced by temperature. The structures of bicontinuous cubic phase are shown in Figure 1.5 (Brown, 2012; Chen et al., 2014; Kaasgaard & Drummond, 2006). In 1960, bicontinuous cubic phases were identified and help in the fusion of biological membrane

and can be used as a templates like synthesis of porous membranes with well-defined structures (Alexandridis et al., 1998).

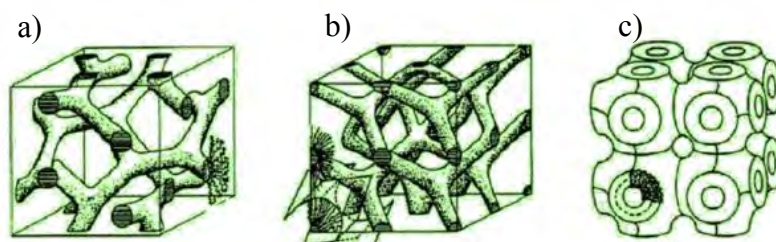


Figure 1.5: Sketch of bicontinuous cubic phase namely (a) $Ia3d$, b) $Pn3m$ and c) $Im3m$ (Redrawn).

The discontinuous cubic phases (I) in lipid/water systems initially with structures composed of spherical aggregates of the type's oil-in-water (normal) or water-in-oil (inverse). In the absence of any directional forces, the arrangement are closely packed face centered and have a long range three-dimensional order crystalline (Fontell, 1990; Fontell et al., 1985). These unique structures may be utilized as a drug delivery. Discontinuous cubic phases (I) consist of discrete micellar aggregates that packed in a cubic array and can be found in some systems, including biological ones, between the isotropic aqueous solution and the hexagonal phase (Rodríguez & Kunieda, 2000). The discontinuous cubic phase consists of the micelles arranged in a cubic lattice, which can be either a face-centered cubic or a body-centered cubic (see Figure 1.6) (Rajabalaya et al., 2017).

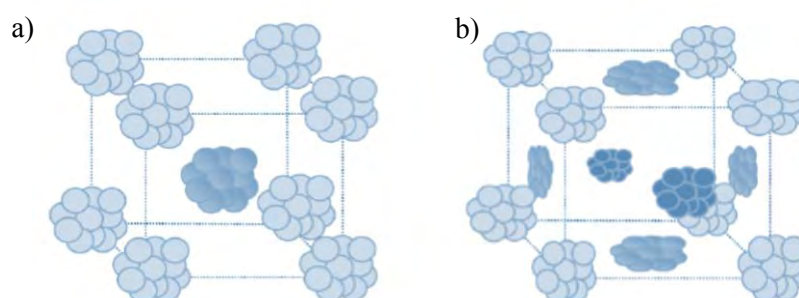


Figure 1.6: Structures of discontinuous cubic namely, (a) body-centered cubic and (b) face-centered cubic (Redrawn).

1.3 Order Parameter

In describing the self-assembly phenomena, the concept of an orientational order parameter is vital as it governs the anisotropic properties. The description of a liquid crystal phase usually involves the analysis of its ordering. For example the simplest order parameter in the nematic phase can be defined as the average of the second-rank Legendre polynomial in the following equation (Equation 1.1) (Vicari, 2003):

$$S = \langle P_2(\cos \theta) \rangle = \left\langle \frac{3}{2} \cos^2 \theta - \frac{1}{2} \right\rangle, \quad \text{Equation 1.1}$$

where θ is the angle between the orientation of the molecular long axis and the director, \mathbf{n} and $\langle P_2(\cos \theta) \rangle$, is the average second-order Legendre polynomial. This average is taken over an ensemble of molecules. Figure 1.7 illustrates the schematic diagram of a nematic phase.

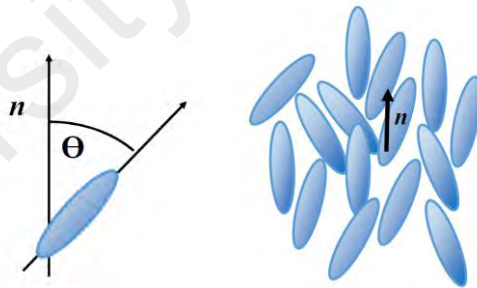


Figure 1.7: The schematic diagram of a nematic phase where molecules are distributed about the local director $\uparrow \mathbf{n}$, θ is the angle between the molecular long axis and the director (Redrawn).

In a smectic phase, there are two order parameters, for position and orientation, respectively. The orientational order in smectic closely resembles that of a nematic. On the other hand a positional order parameter is characterized by the variation of the density of the center of mass of the liquid crystal molecules along a given axis. The positional variation along the z -axis of the density $\rho(z)$ is often given by:

$$\rho(r) = \rho(z) = p_0 + p_1 \cos(q_s z - \varphi) + \dots \quad \text{Equation 1.2}$$

The complex positional order parameter is defined as $\psi(r) = p_1(r)e^{i\varphi(r)}$ and p_0 the average density. Typically only the first two terms are kept and higher order terms are ignored since in most phases this can be described adequately using sinusoidal functions. For a perfect nematic $\psi = 0$ and a smectic phase ψ will take on complex form. In McMillan model of a smectic A, the positional order parameter is given as:

$$\sigma = \cos\left(\frac{2\pi z_i}{d}\right) \left(\frac{3}{2} \cos^2 \theta_i - \frac{1}{2}\right), \quad \text{Equation 1.3}$$

where the values z_i , θ_i , and d are the position of the molecule, the angle between the molecular axis and director, and the layer spacing, respectively.

1.4 Curvature Forces in Lipid Interaction

The study of biological membranes seems to be helpful continuously at the localized spontaneous curvature of their constituent monolayers through the curvature forces in lipid interaction. The idea of spontaneous curvature had been proposed by Helfrich and Gruner in 19th century which had attributed the phase structure to a molecular shape by focusing on the range of monolayer curvature that minimizes the bending elastic free energy (Szule et al., 2002). In the aqueous environment, isolated lipid can assemble in various structure. Lipid which have overall cylindrical shape when the cross-sectional area of the headgroup is similar to the cross-sectional area of the chain favour to assemble into a lamellar phase similar to the phase of a biological membrane (Killian & Kruijff, 2004). When the cross-sectional area of lipid head group is larger than that of the hydrocarbon chain, it will forms a positive curvature (Type I lipids). For example lipids with positive curvature will tend to form micelle in water. On the other hand, when the

cross-sectional of the head group is smaller, aggregate structures with a negative curvature (Type II lipids) are preferred such as inverse hexagonal phase (Brown, 2012; Killian & Kruijff, 2004).

University of Malaya

CHAPTER 2: LITERATURE REVIEW

2.1 Natural Glycolipid

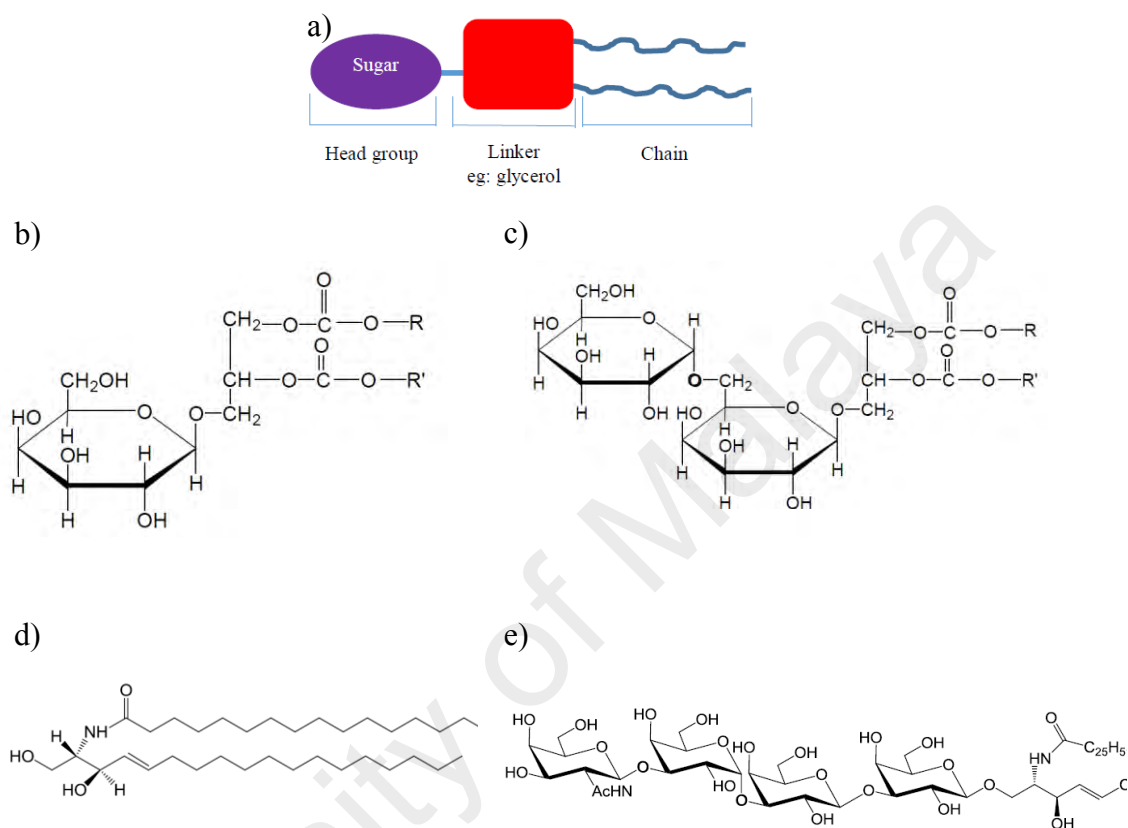


Figure 2.1: Natural glycolipid: (a) typical structure and some examples: (b) monogalactosyl-diacylglycerol (MGDG) (c) digalactosyldiacylglycerol (DGDG) (d) ceramide (e) β -hexosaminidase (Redrawn).

A natural glycolipid contains a carbohydrate unit linked to a lipid, for examples acylglycerols and ceramides (see Figure 2.1). The structures of natural glycolipids are amazingly complex as these may have tremendous varieties of possible coupled carbohydrate residues and the number of connected hydrocarbon chains (Garidel et al., 2015). Glycolipids can also be synthesized and these may give liquid crystalline phases (Vill & Hashim, 2002). In addition, glycolipids display thermotropic and when dissolved in solvent like water, they also form the lyotropic phases. Hence the term amphitropic

applies to glycolipids (see Baron for IUPAC nomenclature) (Baron, 2001; Ewing et al., 1997; Garidel et al., 2015).

Glycolipids have gained so much interests since these are connected with the membrane functionality and believed that they involve in molecular recognition on cell surfaces and stabilization of the membrane structures, for example glycolipids for natural killer T-cell (Hato & Minamikawa, 1996; Savage, Teyton, & Bendelac, 2006). They are environmentally friendly, biodegradable and less toxic, hence they are widely used in many applications (Pacwa et al., 2011). For example, commercially available alkyl glucosides have been used in the fields of cosmetics due to their excellent behaviour at the interfaces which make them useful in the preparation of microemulsions, detergents and pesticide formulations (Messinger et al., 2007; Rather & Mishra, 2013; Schmid & Tesmann, 2001).

Highly pure natural glycolipid are difficult to extract and their total synthesis often proves challenging, which makes synthetic substitutes become increasingly in demand (Liew et al., 2015). Previously, a class of branched chain glycolipid with different total alkyl chain length already been studied for their properties with different headgroups like glucose, galactose, maltose and xylose (Hashim et al., 2011; Liao et al., 2006; Liew et al., 2015).

2.1.1 Guerbet Glycolipids

In order to mimick these natural lipids, a class of branched chain glycolipid has been synthesized using different types of sugars from mono- and disaccharides (glucose, galactose, maltose and lactose) and Guerbet alcohols as a precursors. These alcohols are branched at the 2- or β -position and were first prepared by Marcel Guerbet (Hashim et al., 2012). Guerbet branched-chain glycolipids can be viewed as Guerbet sugars, which add to the collection of Guerbet compounds including Guerbet alcohols, acids and esters

(Knothe, 2002). In general, Guerbet alcohol refers to highly branched, saturated alcohols prepared by the condensation of two primary alcohols and these products are significant in the production of surfactants because of their low irritation potential, low volatility and reactive. Guerbet alcohols have become useful in the production of surfactants because of their low irritation potential, low volatility and reactive (Kozlowski & Davis, 2013; O'Lenick Jr, 2001).

2.1.2 Mannose Base Glycolipids

The term mannose comes from the word *manna*, which is frequently used in the Bible and means an unknown sweet secretion. It also can be named as D-mannosies and the chemical formula is $C_5H_{11}O_5CHO$ (Hu et al., 2016). Mannose is a monosaccharide or a simple sugar because it cannot be hydrolyzed to other forms of carbohydrate. Besides, mannose is readily soluble in water and has a characteristic sweet flavor (Daley & Daley, 2017; Rojas, 2016). In addition, mannose is chiral in the ring form but achiral in linear form (Fu et al., 2006; Mosapour Kotena et al., 2014). Mannose is an aldohexose group which can be found in nature from many fruits such as cranberries. It is an epimer of glucose and differ at the C2 position where the hydroxyl group OH is axially oriented (Figure 2.2) (Hu et al., 2016; Mosapour Kotena et al., 2014). Mannoside is a glycoside of mannose. It is often assumed that mannosides play key roles in metabolism, cell recognition, and can be involved in many diseases like the prevention and the treatment of urinary tract infections (Ladeveze et al., 2017; Mosapour Kotena et al., 2014). Figure 2.2 shows the structure of mannose and compare with other sugars.

Understanding the process of liquid crystal provide a deeper insight and appreciation of the biological functionality. The present research employs different branched alkyl chain glycolipids based on mannose as the head group. It should be noted that previously, a study on mannose by using the octyl- α -D-mannofuranoside have shown the smectic A behaviour (Goodby et al., 2007). Additionally, sugar headgroups are very important in controlling the phase hence the application behaviour. By using mannose as the headgroup in these lipids, some new liquid crystalline properties may be elucidated.

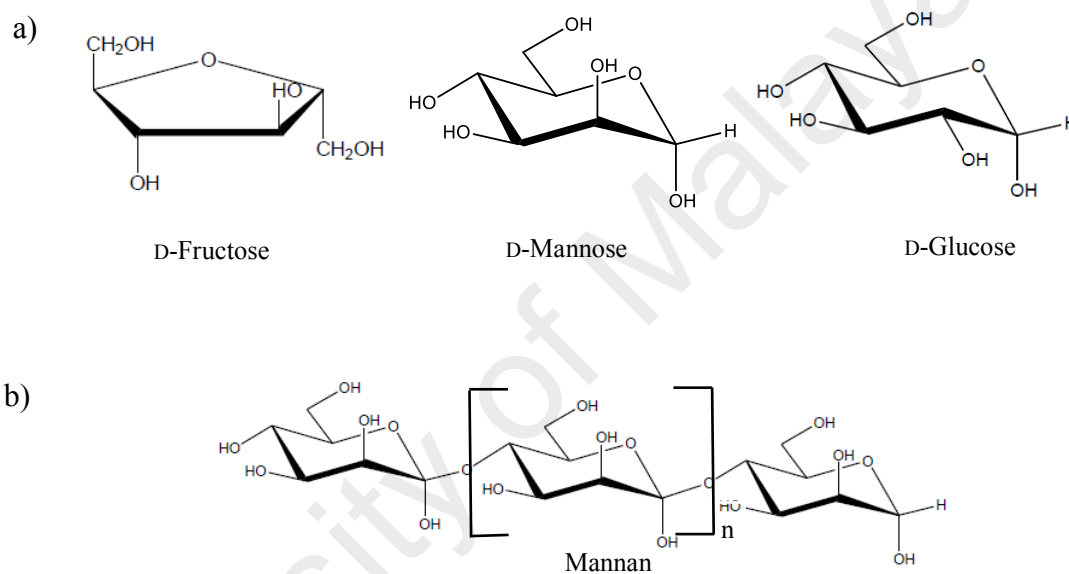


Figure 2.2: Chemical structures of D-mannose (a) comparing mannose with glucose and fructose (b) polymer of mannose (Hu et al., 2016) (Redrawn).

2.2 Objectives of Study

In understanding the glycolipid materials and their potential applications, this research investigates the branched chain Guerbet glycolipids. These types of glycolipids have proved to mimic closely their corresponding natural products (Vill & Hashim, 2002). Guerbet branched alkylated hydrophobic tail which contains two asymmetric chain ranging from C₆C₂, C₈C₄, C₁₀C₆, C₁₂C₈ and C₁₄C₁₀. To achieve in understanding of these glycolipids liquid crystalline phases, the following objectives have been targeted:

- i. to synthesis a series of glycolipids namely α -D-mannopyranoside with different branched alkyl chain lengths
- ii. to characterize the thermotropic and lyotropic phase behaviour using optical polarizing microscopy (OPM) and differential scanning calorimetry (DSC)
- iii. to determine the size structure of the parameters of the mesophases and by small angle X-ray scattering (SAXS)

CHAPTER 3: METHODOLOGY

3.1 Synthesis of Guerbet Mannosides

The importance of oligosaccharides in many biological and pharmaceutical processes has motivated the development of many glycosylation methods over the last two decades. For example, glycolipids assume a critical part in cell processes such as endo- and exocytosis, cell death and molecular recognition at the cell surface (Sasaki, 2008). Due to the richness of carbohydrate chemistry, many new synthetic procedures were developed to create a glycosidic bond between sugar head and hydrocarbon chain (Boons, 1996; Davis, 2000; Schmidt, 1986; Schmidt & Kinzy, 1994; Yu & Tao, 2001). The stereoselective synthesis of *O*-glycosidic bonds is the key to study their role of the biological systems (summarized in Scheme 3.1) (Johansson, 2015). In 1890, Emil Fischer developed the first glycosylation method using sugar and alcohol in the presence of hydrochloric acid (Villardier & Corma, 2010). There are other glycosylation methods such as Koenigs-Knorr reaction. This reaction is widely used for the preparation of alkyl glycosides in which sugars were first acetylated and converted to brominated peracetate in the presence of Lewis acid activator, for example, SnCl_4 , Tf_2O and TrClO_4 (Koeltzow & Urefer, 1984; Toshima, 2006). Following this, the deacetylation was carried out using sodium methylate (Koeltzow & Urefer, 1984). The chemical structure of glycosyl halide, alcohol, activator used and the solvent will influence the yield and the product composition (Garegg et al., 1985).

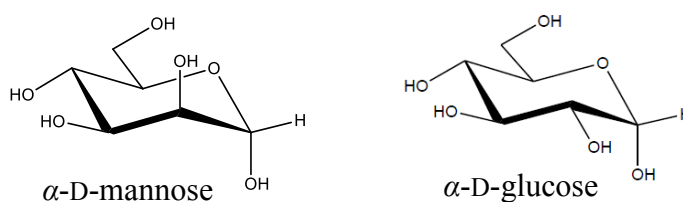
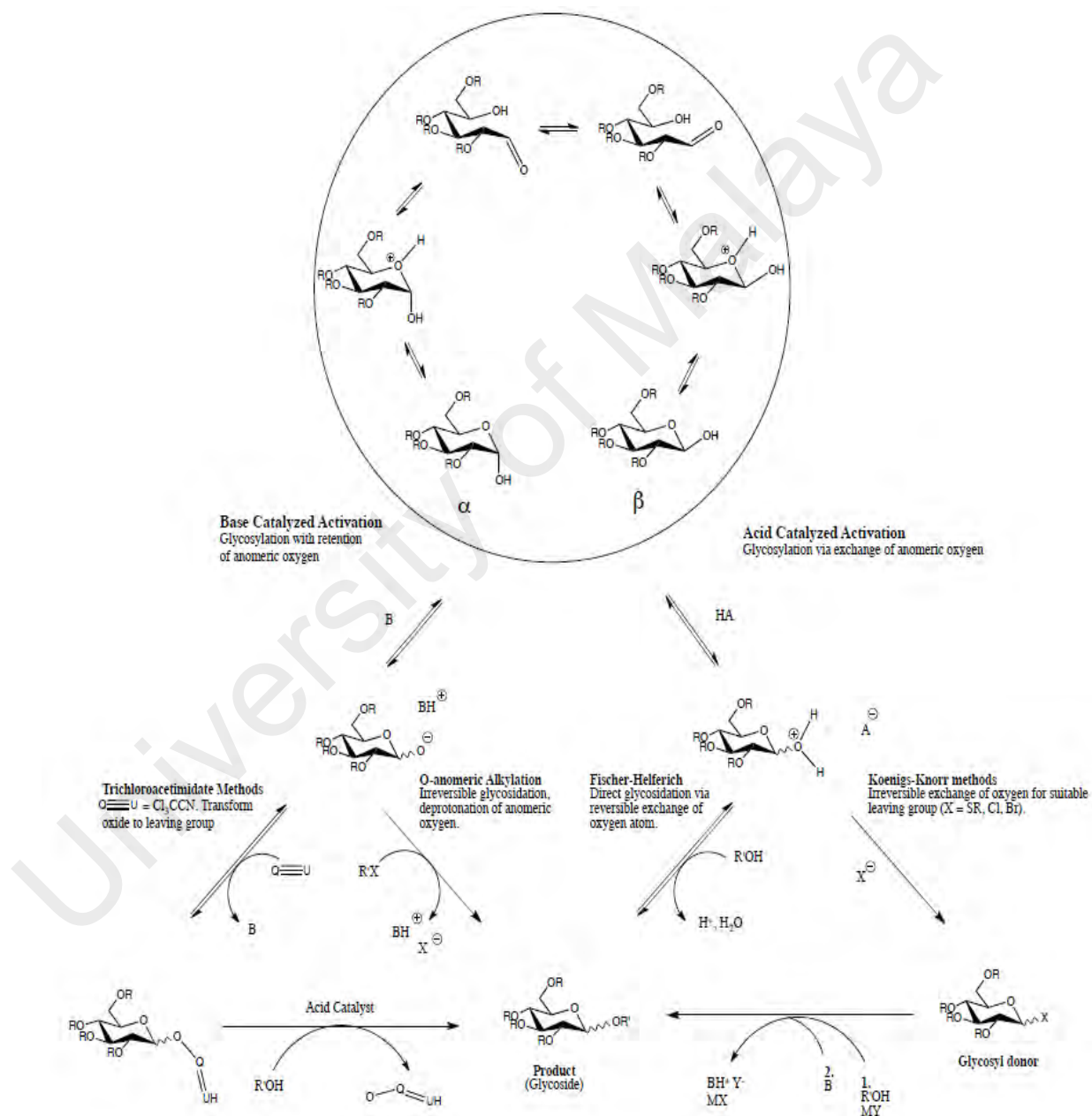


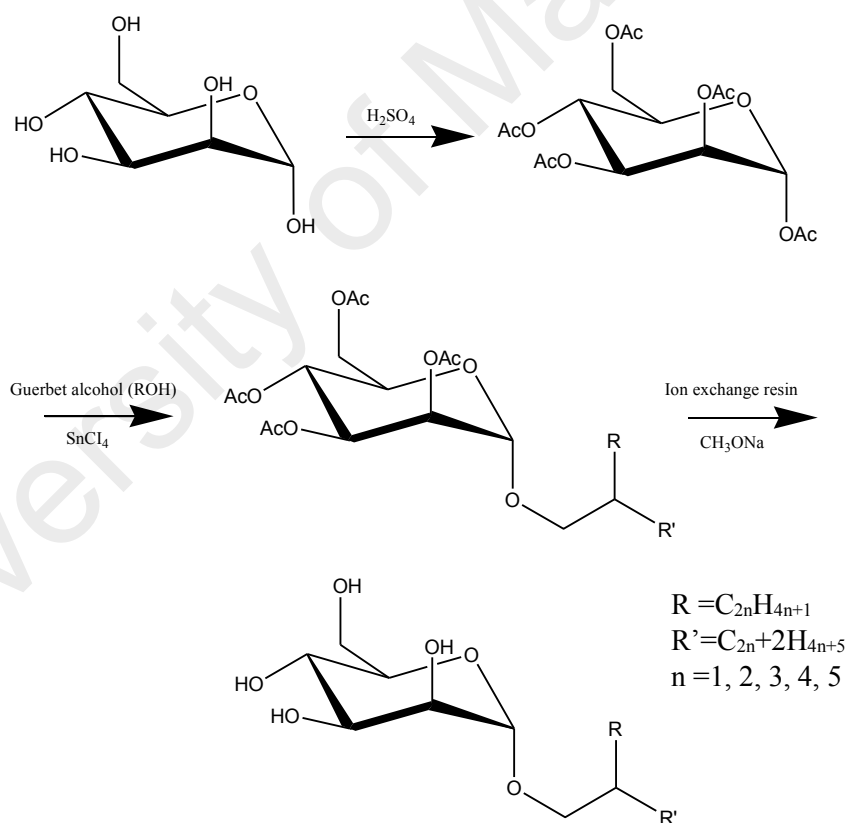
Figure 3.1: Different hydroxyl (-OH) group of mannose and glucose at C2 position

This work focuses on alkyl mannosides which are synthesized by a chemical glycosylation reaction between D-mannose as the sugar head group and a series of Guerbet alcohols as the lipid tails. D-mannose, a C2 epimer of D-glucose, differs from the latter at the second carbon atom, where the hydroxyl group is axial (for mannose) and equatorial (for glucose) as shown in Figure 3.1 (Mosapour Kotena et al., 2014).



Scheme 3.1: Overview of general glycosylation methods (Johansson, 2015).

Basically, the Guerbet mannosides can be synthesized in three steps involving: the peracetylation reaction to protect hydroxyl (-OH) group on sugar; the glycosidation reaction to attach the Guerbet alcohol to the sugar head group via an ether linkage using tin tetrachloride in dichloromethane (Polakova, 2010) and finally, the highly pure glycolipids undergo deacetylation reaction with sodium methylate as catalyst in basic medium to remove all acetate protecting groups. In the glycosidation process, the catalyst and later the product can be purified by column chromatography. The anomeric purity can be determined by ¹H-Nuclear Magnetic Resonance (NMR) spectroscopy (Vill et al., 1989). The brief reaction scheme for synthesis is shown in Scheme 3.2.



Scheme 3.2: Reaction scheme to synthesize Guerbet mannose glycolipids series.

3.1.1 Materials

The starting mannose sugar, D-(+)-Mannose (99%), five Guerbet alcohols (97%), of total chain length C₈, C₁₂, C₁₆, C₂₀, C₂₄ and Tin (IV) chloride solution, 1.0 M in methylene chloride were obtained from Sigma-Aldrich. Sodium methylate (97%), ACS grade solvents including dichloromethane, acetonitrile, ethyl acetate, *n*-hexane and methanol were supplied from Merck. These were used as supplied without further purification.

Thin layer chromatography (TLC) was developed on silica gel purchased from Merck coated on aluminum plates and immersing it in the solution of the mixture ethanol, water and sulfuric acid (90:8:2) in the chamber followed by heating using heat gun.

Flash column chromatography was done on silica gel 60 from Merck with pore size 35–70 μm (stationary phase). *n*-hexane and ethyl acetate mixture was used as the mobile phase. A moderate pressure was applied to the column chromatography to ensure consistent flow of eluent by using a bellow pump.

The chemical structure and anomeric property of the synthesized compounds were characterized by ¹H- and ¹³C- NMR spectroscopy. NMR spectra were confirmed at room temperature on Bruker Avance 400 NMR spectrometer that located in the Department of Chemistry, University of Malaya. Two types of deuterated solvents were used for chemical characterization namely chloroform-d for the protected glycolipids and methanol-d₄ for the deprotected glycolipids. The residual solvent peaks were set for chloroform-d at 7.26 ppm for ¹H-NMR and 77.23 ppm for ¹³C-NMR. For methanol-d₄, the reference was set at 4.87 ppm and 49.15 ppm for ¹H-NMR and ¹³C-NMR, respectively.

3.1.2 Characterization using Nuclear Magnetic Resonance (NMR)

NMR spectroscopy is widely used in the study of carbohydrate chemistry. It has become a part of the standard methodology in order to characterize the glycoprotein carbohydrates. Other than that, these was used to obtain the physical, chemical, electronic and the structural information about the molecule as well as for the undergoing chemical reactions (Darbeau, 2006). It was determined by the result with a chemical shifts of spectra which was used to determine the molecular structure. Deuterated solvents will be added to the sample for the magnetic field stability and shimming (Nanda & Damodaran, 2018). NMR spectroscopy is quantitative and does not require extra steps for sample preparation, such as separation or derivatization (Emwas, 2015).

Measurement

^1H - and ^{13}C -NMR spectra were recorded in Bruker FT-NMR Avance III 400 MHz. TopSpin software was used to get the signal of NMR spectra. The spectra were labeled as follows: s (singlet), d (doublet), dd (doublet to doublet), ddd (doublet of doublet of doublet), t (triplet) and m (multiplet). NMR tubes (5mm) was used and two types of deuterated solvents were used for chemical characterization namely chloroform-d for the protected glycolipids and methanol-d₄ for the deprotected glycolipids.

3.1.3 General Peracetylation Procedure: Synthesis of α -mannose pentaacetate

D-mannose (4.98 g, 27.8 mmol) in acetic anhydride (27 mL, 286 mmol) was set up in a round bottom flask and stirred in the ice bath for 15 min. At that point, it was catalysed by concentrated sulphuric acid (2 drops) and was additionally stirred on the ice bath (10 min). The mixture was then permitted to warm at room temperature under stirring for an additional 45 min. Afterward, the mixture was moved into a separating funnel and diluted with ice water (100 mL) and extracted with ethyl acetate (100 mL). The extraction was

reashed 3 times by washing the mixture with the ice water. Then the organic layer was quenched with saturated hydrogen carbonate solution twice. The extract was dried with anhydrous magnesium sulphate (MgSO₄), sifted and evaporated. Their chemicals structured were confirmed by ¹H- and ¹³C-NMR spectra.

3.1.4 General Glycosidation Procedure: Synthesis of α -alkyl mannosides

α -mannose pentaacetate (5 g, 12.8 mmol, 1.0 equiv.) was mixed into dichloromethane (200 mL) and the temperature of the solution was cooled down toward 5°C on an ice bath. Then, 1 M tin tetrachloride (12.8 mL, 69 mmol, 5.4 equiv.) was added into the solution via a syringe as a catalyst. The solution was stirred for 10 min and afterward, the corresponding Guerbet alcohol (2.5 mL –6.5 mL, 15.4 mmol, 1.2 equiv.) was added dropwise. The mixture was stirred for another 15 min and conveyed to room temperature. The mixture was left for 16 h under stirring. The progress of reaction was observed by TLC (hexane: ethyl acetate, 2:1). After the reaction completed, it was diluted with 200 mL dichloromethane and dispensed into ice cold saturated sodium hydrogen carbonate (50 mL) under stirring. The organic layer was separated, washed with water, dried over anhydrous MgSO₄, filtered and concentrated. The product was further separated via hexane –acetonitrile system to remove the excess alcohol. The acetonitrile layer was separated and evaporated. The crude product was purified by column chromatography (hexane-ethyl acetate, 5:1). Their chemical structures were confirmed by ¹H- and ¹³C-NMR spectra.

3.1.5 General Deacetylation Procedure

The product from the previous stage was dissolved in methanol (1 g in 30 mL). A catalytic amount of sodium methoxide was added into the flask to make the solution basic. The solution mixture was stirred overnight. After the reaction completed, the solution was

neutralized with H⁺ ion exchange resin (Amberlite IR-120), filtered and evaporated. The solvent was evaporated and the remaining product was dried over di-phosphorus pentoxide for 48 h under vacuum. Their chemical structures were confirmed by ¹H- and ¹³C-NMR spectra.

3.2 Liquid Crystal Phase Behaviour

There are several techniques used to characterize the liquid crystal phase behaviour. Generally, identification of liquid crystal phases was conducted by a combination of techniques involving the Fourier transform infrared spectroscopy (FTIR), differential scanning calorimetry (DSC), the optical polarizing microscopy (OPM) and the small angle X-ray scattering (SAXS).

3.2.1 Fourier transform infrared spectroscopy (FTIR)

Fourier transform infrared spectroscopy (FTIR) is a non-dispersive method of infrared spectroscopy. It measures all infrared frequencies simultaneously via interferometer and the sample can be analyzed by either transmittance or reflectance mode (Thomas, 2008). This spectroscopic technique is simple, reproducible and only use a small amounts of material for identification of material's type of bonds and molecular conformations (Movasaghi et al., 2008).

Measurement

Infrared spectrum of absorption for α -D-mannose were identified by using Spectrum 400 FTIR Spectrometer. The Spectrum ES 10TM software was used to control the instrument and to manipulate the spectra. Since glycolipids are hygroscopic, the samples were first desiccated in a vacuum oven over di-phosphorus pentoxide for no less than 48 h before the measurement. Transmission FTIR spectroscopy was the method employed

for this study. Data analysis is performed by assigning the observed absorption frequency bands in the sample spectrum to appropriate normal modes of vibrations in the molecules.

3.2.2 Differential Scanning Calorimetry (DSC)

Calorimetry is applied to measure the heat effects that happen in physical, chemical or natural related processes by the study of the enthalpy changes in relation to pressure and temperature. Calorimetry data is interesting to researchers in this field (Demetzos, 2008), since it involves the study of the phase transitions of molecules using heat flux from calorimeter (Wunderlich et al., 1999). DSC is a complementary tool to OPM. It becomes useful since only a small size of the sample is required. It has a high sensitivity to reveal the presence of liquid crystal phase which depend on the sample and the rate of scanning (Mazzobre et al., 2003). This technique involves the measurement of the heat flux (thermal power) to and from the sample against time or temperature. The temperature of the sample is programmed in a controlled atmosphere. The difference of heat flux between a crucible containing the sample and a reference crucible (empty or not) is measured (Auroux, 2013).

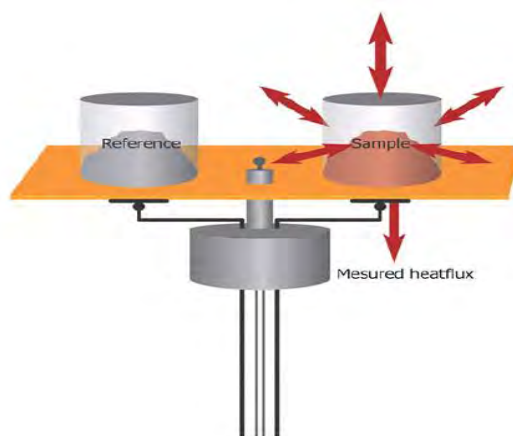


Figure 3.2: Principle of heat flux (Auroux, 2013).

As shown in Figure 3.2, both reference and sample are placed in the crucible on a sample holder. The heat generated will flow towards the samples. A minimum of three measurements is necessary to obtain the specific heat. Initially, in order to remove the system bias, a “baseline” measurement is made in which both crucibles empty. Then a sample with a specific heat will be tested for a comparison with an experimental sample. The reference test will give a calculation for the specific heat with the experimental sample as a ratio of the reference material specific heat (Daw, 2008).

Measurement

Phase transition temperature for the mannosides were identified with a DSC Mettler Toledo 822° equipped with Haake EK90/MT intercooler. Star° Thermal Analysis System software was used for data analysis. Sample weighing between 4–8 mg was placed in a sealed crucible pan. The heat and enthalpy accuracy were tested by using indium metal and an empty pan as a reference for the calibration. The experiments were performed for both heating and cooling cycles. Since glycolipids are hygroscopic, the samples were first desiccated in a vacuum oven over di-phosphorus pentoxide for no less than 48 h before being encapsulated in the crucible pan. Each sample was heated $10^{\circ}\text{C min}^{-1}$ and scanned from -40°C up to 150°C . The transition results was recorded as heat flow versus temperature.

3.2.3 Optical Polarizing Microscopy (OPM)

The other techniques to characterize liquid crystals phase is by optical polarizing microscopy. Since liquid crystals are anisotropic, the polarized light along and perpendicular to the director travel at a different velocity. Under a crossed polarizer the anisotropic nature of the liquid crystal make the medium appear bright or birefringence

(An et al., 2016). An optical polarizing microscope allows the determination of phase identity as well as the nature of phase is characterized by a particular observed texture due to the presence of defects within the phase. Melting point transition from one phase to another and clearing point of liquid crystal can also be observed by using optical polarizing microscope. Figure 3.3 shows the components parts of optical polarizing microscope.

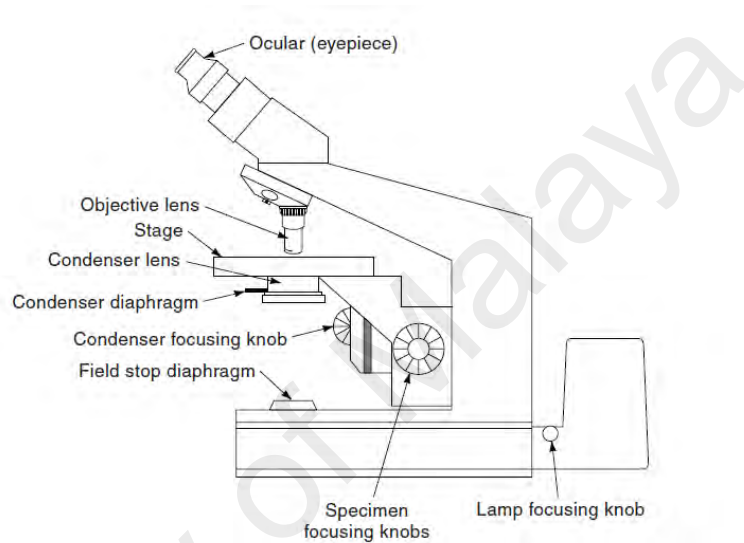


Figure 3.3: Components parts of optical polarizing microscope (Murphy, 2002).

In forming the image, there are two important components, namely the objective lens that collects lights diffracted by the specimen to form the magnified real image. Secondly, the condenser lens that focuses the light from the illuminator onto a small area of the specimen. A simplified scheme of how the image is formed is shown in Figure 3.4. In this figure, an image is magnified by the objective lens and is captured by the eyepiece (ocular) to produce the real image. It was recorded directly or projected as a real image onto a camera (Murphy, 2002).

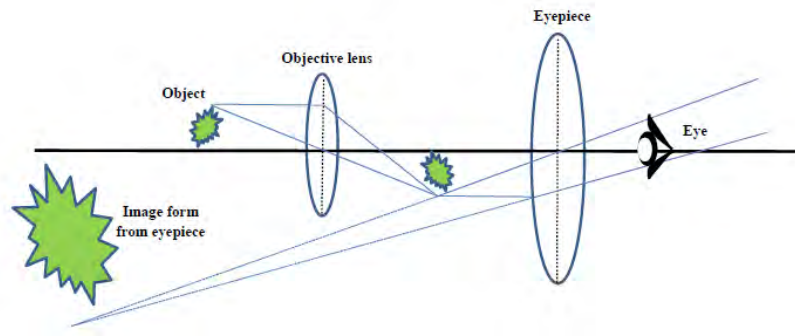


Figure 3.4: An image that magnified in the microscope (Redrawn).

Birefringent crystals such as liquid crystals appear bright when viewed through crossed polarizers depending on their velocities, the waves that get out of phase by passing through the individual polarizers (called ‘analyzer’). Polarization refers to limitations on the direction of wave oscillation. A polarizer acts like a filter to allow only light oscillating in one orientation to pass. When the polarized light interacts with the sample that contrast with the background, birefringent are always appear. Polarized light is capable to give information on optical path boundaries within the sample structures as well as can differentiate between the isotropic and anisotropic samples. It always gives a unique internal structure of crystals by showing coloured texture and the shape of the crystals (see Figure 3.5) (Carlton, 2011; Voelker-Pop, 2014).

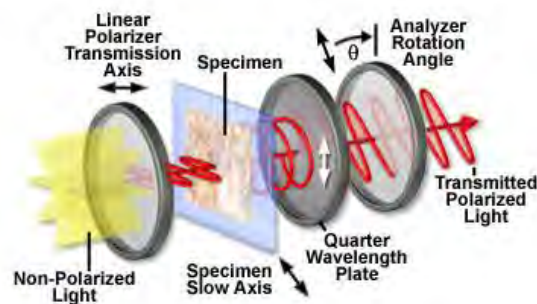


Figure 3.5: Basic principle of optical polarizing microscope (“Microscope Primer”, 2017).

Thermotropic Phase Behaviour

In order to investigate the thermotropic phase behaviour of a liquid crystal, the sample was desiccated in a vacuum oven in excess of di-phosphorus pentoxide for at least 48 h. Dry sample was placed on top of the glass slide and a cover slip is used to cover the sample as shown in Figure 3.6. The heating stage was then used to heat the sample from room temperature until it became isotropic phase. Subsequently, it was cooled to room temperature at the rate of $5^{\circ}\text{C min}^{-1}$. This step ensures a uniform thickness and remove all the remnant crystallinity within the sample. A second heating was applied to determine the phase transition temperature until it reached the isotropic phase. The liquid crystal images were captured as it forms the clear optical textures while it cooled down at the rate of $1^{\circ}\text{C min}^{-1}$.

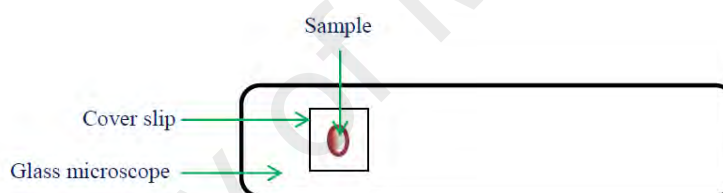


Figure 3.6: Preparation of sample onto the glass microscope (Redrawn).

Lyotropic Phase Behaviour

Lyotropic behaviour was studied qualitatively using the contact preparation method. As in the thermotropic study, the sample is placed on top of glass slide. The sample is heated until isotropic before cooled to room temperature. Then a drop of water was introduced at the edge of the cover slip to allow contacting with the sample. The water moves under the glass slip by capillary action to form a concentration gradient that ranged from pure water to neat sample towards the middle as shown in Figure 3.7.

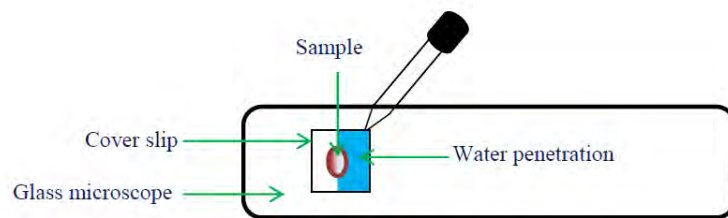


Figure 3.7: Contact preparation used for the study of lyotropic behaviour (Redrawn).

Measurement

The liquid crystalline phases of mannosides were identified by using Mettler Toledo Mettler Toledo FP90 Central Processor (Figure 3.8) together with FP82HT hot stage (Figure 3.9) connected to an Olympus BX51 camera. The transition temperature of the sample was identified by using the hot stage controller to control the heating and cooling measurement. The image of the texture was captured to the Olympus camera and cellSens standard software was used for image analysis and storage.



Figure 3.8: Mettler Toledo FP90 central processor (“Mettler Toledo”, 2017).



Figure 3.9: Mettler Toledo FP82HT hot stage (“Thermal Microscopy Hot Stage”, 2017).

3.2.4 Small Angle X-ray Scattering (SAXS)

Small angle X-ray scattering (SAXS) technique was employed to determine the structures of liquid crystals and their symmetries. The liquid crystal phase that had been determined by OPM, was confirmed by the SAXS measurement. OPM allows the visualization of the texture of a particular liquid crystal phase since a different liquid crystal phase gives a distinct texture pattern. On the other hand, the SAXS technique is used to analyse the structure of the phases from the scattered radiation of the repeat distances within the structure (Pauw, 2011). The sample can be analyze using two main approaches namely the line collimation and point collimation. The resolution of the measurement is within the range of 1 to 100 nm (Schnablegger & Singh, 2011). The instrument has their own components which are important in the scattering measurement which are X-ray source, collimator, sample holder, and detector. The X-ray beam will illuminates the sample in the sample holder where it focused by the collimator. The spatially coherent beam interacts with the sample and is scattered by an angle 2θ , and then travels toward the detector (Venditti et al., 2016). Then, the X-ray detector will record the scattering and give a reflection pattern typified of the structure of self-assembly (Kikhney & Svergun, 2015). As shown in Figure 3.10, the setup of SAXS experiment required a collimated monochromatic X-ray beam that will illuminate the sample in the sample

holder. The characterization of liquid crystal phases is due to the presence of the long range order within the liquid crystalline phase which give rise to a distinctive set of Bragg's reflections (Nilsson et al., 1996).

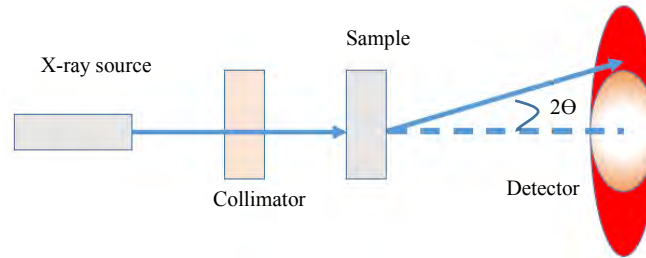


Figure 3.10: The setup of X-ray scattering experiment (“Dimensional Metrology for Nanofabrication”, 2009) (Redrawn).

The discovery of Bragg's Law have gained its popularity to study the liquid crystal. (Figure 3.11 and Figure 3.12). The condition for valuable interference that the beam reflected from adjacent lines ought to vary in way length by an integral number, n , of wavelengths, then simply bring to the Bragg equation (Pope, 1997):

$$n \lambda = 2d \sin \theta \quad \text{Equation 2.1}$$

where λ is the wavelength of the rays, θ is the angle between the incident rays and the surface of the crystal, d is the spacing between layers of atoms and constructive interference occurs when n is an integer (whole number).

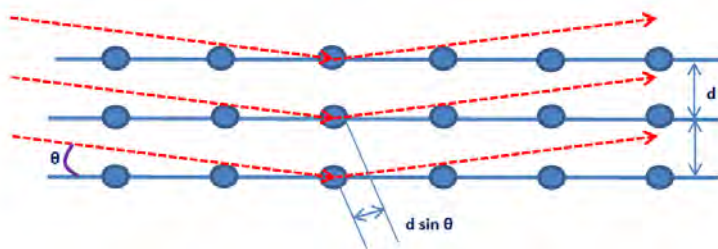


Figure 3.11: Bragg expressed for SAXS at 7° (Werneck et al., 2013).

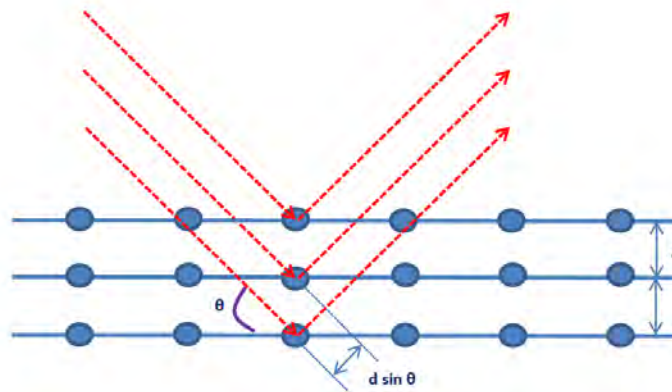


Figure 3.12: Bragg expressed for WAXS at 45° (Werneck et al., 2013).

The scattering pattern is usually presented as a function q , which is the length of the scattering vector.

$$q = \frac{4\pi \sin\theta}{\lambda} \quad \text{Equation 2.2}$$

where λ is the wavelength of the incident radiation and θ is half the angle between the incident and scattering radiation (Jacques & Trewhella, 2010).

Measurement of X-ray scattering has become a central device in study of the structure compounds. The only difference between the experimental setup for SAXS and WAXS is the scattering angle. The distance of the sample from the detector will effects the range of scattering angles. During WAXS experiments, the detector is placed closer to the sample to collect higher angle scattering data. SAXS generally characterized as a extending to scattering angles that corresponds to spacing of $\sim 15\text{--}20 \text{ \AA}$ ($q \sim 0.3 \text{ \AA}^{-1}$). In contrast, WAXS studies the scatterings angles that resembles to $q \sim 2.5 \text{ \AA}^{-1}$ (Makowski, 2010).

Sample Preparation

Until the day before the measurement, the lyophilized samples were kept in a vacuum desiccator. Excess water were set up at 90% concentration (90% w/w) by adding appropriate amount of water and dry lipid into a 1.5-mL micro centrifuge tube. Homogenization hydration was done by repeating centrifugation and was equilibrated for at least a week before SAXS measurements were made. Approximately 50 mg of sample was transferred to a paste cell holder and loaded into the X-ray machine.

Measurement

The scattering pattern for dry and hydrated samples were characterized by using an analytical small angle X-ray scattering from SAXSpace (Anton Paar, Austria) and it was equipped with an X-ray tube generating Cu-K α radiation ($\lambda=1.542 \text{ \AA}$) at 40 kV and 50 mA. The scattering patterns were recorded on a one-dimensional diode detector in line collimation mode. Silver behenate ($\lambda =58.4 \text{ \AA}$) was used as a calibrant for all measurements. The sample temperature was controlled using a Peltier system (TCStage 150) within an accuracy of $\pm 0.1^\circ\text{C}$.

Approximately 50 mg of the dry samples was put into the paste cell holder and loaded into the X-ray machine. The sample was heated until it become isotropic and left it for overnight before running the experiment. The excess water samples that have reached thermodynamic equilibrium were immediately characterized after loading to the sample holder. Both dry and excess water samples were equilibrated for 30 min at the desired temperature prior to a 1 h acquisition time. Once the measurement completed, the data was analysed by using the SAXStreat software, SAXSquant software and the liquid crystal phases and the corresponding lattice parameter was determined by using SGI software.

CHAPTER 4: RESULTS AND DISCUSSION

Chapter 4 focuses on the results and discussion of the studied compounds. In this work, five branched chain mannosides namely α -Man-OC₆C₂, α -Man-OC₈C₄, α -Man-OC₁₀C₆, α -Man-OC₁₂C₈ and α -Man-OC₁₄C₁₀ have been synthesized and their chemical structures are illustrated in Figure 4.1 by using Chemdraw software. Their thermotropic and lyotropic liquid crystals were characterized by using DSC, OPM and SAXS.

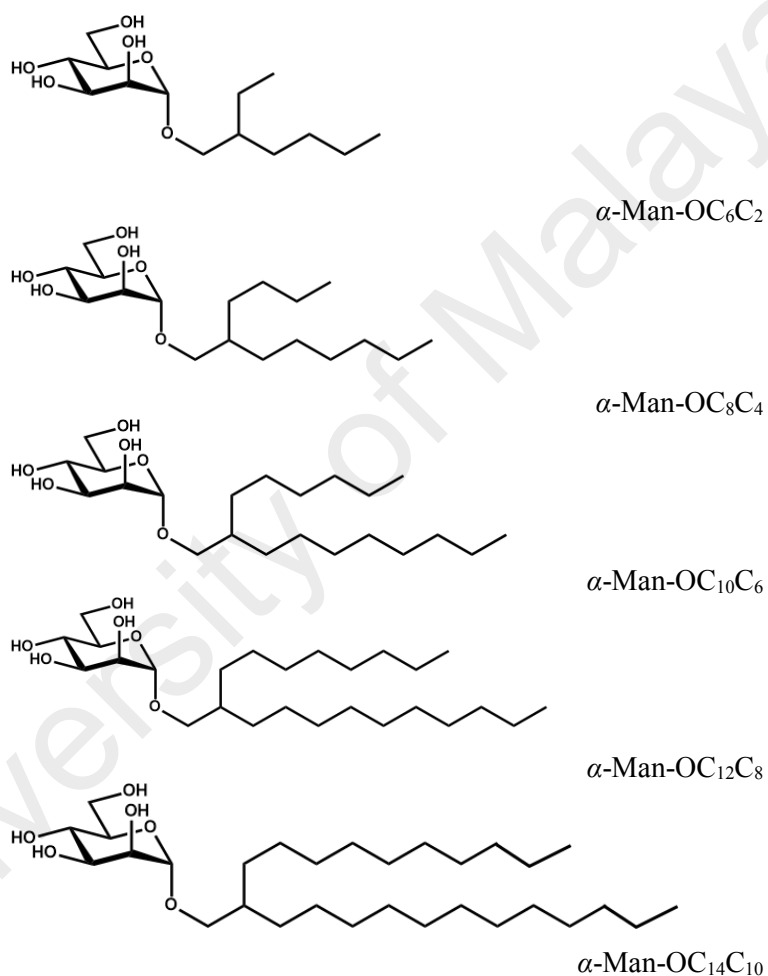
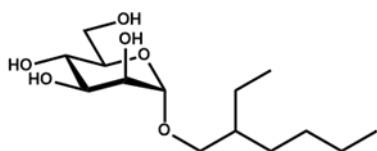


Figure 4.1: The chemical structures of the Guerbet branched α -D-mannosides.

4.1 Synthesis of the Guerbet Mannosides

The detailed synthetic steps of Guerbet mannosides have been described in the previous Chapter 2 which is based on a previously reported procedure (Polakova, 2010). Their anomeric purity was estimated to be $\geq 97\%$ according to $^1\text{H-NMR}$. Both $^1\text{H-}$ and $^{13}\text{C-NMR}$ data for the homologous series of branched chain $\alpha\text{-D-mannosides}$ are given below. Additionally, their $^1\text{H-}$ and $^{13}\text{C-NMR}$ spectra were attached in the Appendix A. Since glycolipids are hygroscopic materials, all the compounds were extensively dried before any liquid crystal phase characterization by keeping the compounds in a vacuum oven over di-phosphorus pentoxide for at least 48 h.

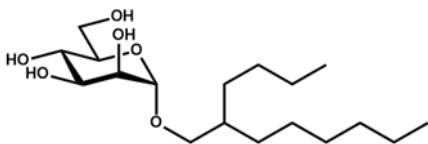
2-ethyl-hexyl- $\alpha\text{-D-mannopyranoside}$, $\alpha\text{-Man-OC}_6\text{C}_2$



$^1\text{H-NMR}$ (400 MHz, CD_3OD): δ (ppm) = 0.90–0.94 (t, 6H, $J = 6.8$ Hz, 2 x CH_3), 1.32–1.50 (m, 8H, CH_2), 1.52 (m, 1H, CH), 3.33 (m, 2H, OCH_2), 3.54 (ddd, 1H, $J_{5,6a} = 2.4$ Hz, H-5), 3.64 (t, 1H, $J_{4,5} = 9.2$ Hz, H-4), 3.68–3.76 (m, 1H, $J_{5,6b} = 5.6$ Hz, H-6b), 3.68–3.76 (m, 1H, $J_{3,4} = 9.2$ Hz, H-3), 3.80 (dd, 1H, $J_{2,3} = 3.2$ Hz, H-2), 3.83 (dd, 1H, $J_{6a,6b} = 11.6$ Hz, H-6a), 4.73 (d, 1H, $J_{1,2} = 1.6$ Hz, H-1)

$^{13}\text{C-NMR}$ (100 MHz, CD_3OD): δ (ppm) = 100.4 (C-1), 73.3 (C-5), 71.3 (C-3), 70.9 (C-2), 69.8 (C-4), 67.2 (OCH_2), 61.5 (C-6), 39.6 (CH), 22.7–30.4 (CH_2), 13.0, 10.1 (CH_3)

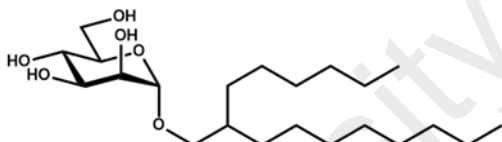
2-butyl-octyl- α -D-mannopyranoside, α -Man-OC₈C₄



¹H-NMR (400 MHz, CD₃OD): δ (ppm) = 0.90–0.94 (t, 6H, J = 6.8 Hz, 2 x CH₃), 1.32–1.50 (m, 16H, CH₂), 1.58 (m, 1H, CH), 3.33 (m, 2H, OCH₂), 3.54 (ddd, 1H, J_{5,6a} = 2.4 Hz, H-5), 3.64 (t, 1H, J_{4,5} = 9.2 Hz, H-4), 3.68–3.76 (m, 1H, J_{5,6b} = 5.6 Hz, H-6b), 3.68–3.76 (m, 1H, J_{3,4} = 9.2 Hz, H-3), 3.80 (dd, 1H, J_{2,3} = 3.0 Hz, H-2), 3.83 (dd, 1H, J_{6a,6b} = 11.6 Hz, H-6a), 4.72 (d, 1H, J_{1,2} = 1.2 Hz, H-1)

¹³C-NMR (100 MHz, CD₃OD): δ (ppm) = 100.4 (C-1), 73.3 (C-5), 71.4 (C-3), 70.9 (C-2), 70.2 (C-4), 67.1 (OCH₂), 61.5 (C-6), 37.9 (CH), 22.3–31.6 (CH₂), 13.0 (CH₃)

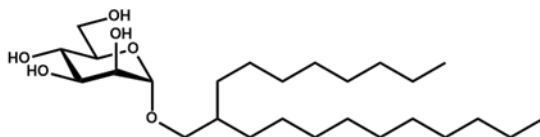
2-hexyl-decyl- α -D-mannopyranoside, α -Man-OC₁₀C₆



¹H-NMR (400 MHz, CD₃OD): δ (ppm) = 0.90–0.94 (t, 6H, J = 6.4 Hz, 2 x CH₃), 1.32–1.50 (m, 24H, CH₂), 1.59 (m, 1H, CH), 3.33 (m, 2H, OCH₂), 3.54 (ddd, 1H, J_{5,6a} = 2.4 Hz, H-5), 3.64 (t, 1H, J_{4,5} = 9.2 Hz, H-4), 3.67–3.76 (m, 1H, J_{5,6b} = 5.6 Hz, H-6b), 3.67–3.76 (m, 1H, J_{3,4} = 9.2 Hz, H-3), 3.80 (dd, 1H, J_{2,3} = 3.2 Hz, H-2), 3.83 (dd, 1H, J_{6a,6b} = 11.6 Hz, H-6a), 4.72 (d, 1H, J_{1,2} = 1.6 Hz, H-1)

¹³C-NMR (100 MHz, CD₃OD): δ (ppm) = 100.5 (C-1), 73.2 (C-5), 71.4 (C-3), 70.9 (C-2), 70.2 (C-4), 67.1 (OCH₂), 61.5 (C-6), 37.9 (CH), 22.3–31.7 (CH₂), 13.0 (CH₃)

2-octyl-dodecyl- α -D-mannopyranoside, α -Man-OC₁₂C₈



¹H-NMR (400 MHz, CD₃OD): δ (ppm) = 0.90–0.94 (t, 6H, J = 6.4 Hz, 2 x CH₃), 1.32–1.50 (m, 32H, CH₂), 1.59 (m, 1H, CH), 3.33 (m, 2H, OCH₂), 3.54 (ddd, 1H, $J_{5,6a}$ = 2.4 Hz, H-5), 3.65 (t, 1H, $J_{4,5}$ = 9.6 Hz, H-4), 3.67–3.76 (m, 1H, $J_{5,6b}$ = 5.6 Hz, H-6b), 3.67–3.76 (m, 1H, $J_{3,4}$ = 9.2 Hz, H-3), 3.80 (dd, 1H, $J_{2,3}$ = 3.2 Hz, H-2), 3.83 (dd, 1H, $J_{6a,6b}$ = 11.6 Hz, H-6a), 4.72 (d, 1H, $J_{1,2}$ = 1.6 Hz, H-1)

¹³C-NMR (100 MHz, CD₃OD): δ (ppm) = 100.5 (C-1), 73.2 (C-5), 71.4 (C-3), 70.9 (C-2), 70.2 (C-4), 67.1 (OCH₂), 61.5 (C-6), 37.9 (CH), 22.3–31.7 (CH₂), 13.0 (CH₃)

2-decyl-tetradecyl- α -D-mannopyranoside, α -Man-OC₁₄C₁₀



¹H-NMR (400 MHz, CD₃OD): δ (ppm) = 0.90–0.94 (t, 6H, J = 6.4 Hz, 2 x CH₃), 1.32–1.48 (m, 40H, CH₂), 1.59 (m, 1H, CH), 3.33 (m, 2H, OCH₂), 3.54 (ddd, 1H, $J_{5,6a}$ = 2.4 Hz, H-5), 3.65 (t, 1H, $J_{4,5}$ = 9.2 Hz, H-4), 3.67–3.76 (m, 1H, $J_{5,6b}$ = 5.2 Hz, H-6b), 3.67–3.76 (m, 1H, $J_{3,4}$ = 9.6 Hz, H-3), 3.80 (dd, 1H, $J_{2,3}$ = 3.6 Hz, H-2), 3.83 (dd, 1H, $J_{6a,6b}$ = 11.6 Hz, H-6a), 4.72 (d, 1H, $J_{1,2}$ = 1.6 Hz, H-1)

¹³C-NMR (100 MHz, CD₃OD): δ (ppm) = 100.5 (C-1), 73.2 (C-5), 71.4 (C-3), 70.9 (C-2), 70.2 (C-4), 67.1 (OCH₂), 61.5 (C-6), 37.9 (CH), 22.4–31.7 (CH₂), 13.1 (CH₃)

4.2 Liquid Crystal Phase Behaviours of Guerbet Mannosides

4.2.1 Thermotropic Phase Behavior

The term “dry” is used rather loosely because the removal of the last trace of water is challenging in sugar lipids (Loewenstein & Igner, 1991). Thus, we have qualitatively determined the degree of water content in these lyophilized (dry) lipids by observing the water stretching and bending modes using the Fourier Transform Infrared Spectroscopy (FTIR). The typical FTIR spectra of the dry lipids (from α -Man-OC₁₄C₁₀) are shown in Figure 4.2(a). The FTIR spectra of lipids that are left at room temperature for 96 h (ambient moisture) and lipids in excess water are included for comparison. The result reveals that in the stretching region ($\sim 3600\text{--}3200\text{ cm}^{-1}$), the IR peak from the dry sample is smaller compared to the other two systems. It should be noted that the broad peak in this region also due to stretching vibration of the –OH group of the lipid. In addition, the water bending mode ($\sim 1700\text{--}1600\text{ cm}^{-1}$) is almost negligible for the dry lipid compared to the other two, implying that our assumption of the “dry lipid” is reasonable. For comparison, Figure 4.2(b) gives the FTIR spectrum of pure water; the O-H stretch band is around ($\sim 3200\text{--}3400\text{ cm}^{-1}$) corresponding to symmetric and asymmetric stretching mode of water, the overtone bands ($\sim 1900\text{--}2500\text{ cm}^{-1}$) and the bending mode ($\sim 1400\text{--}1800\text{ cm}^{-1}$).

The thermotropic liquid crystalline behaviour of five Guerbet α -D-mannosides whose chain length varies from α -Man-OC₆C₂, α -Man-OC₈C₄, α -Man-OC₁₀C₆, α -Man-OC₁₂C₈ to α -Man-OC₁₄C₁₀ were studied using DSC, OPM and SAXS.

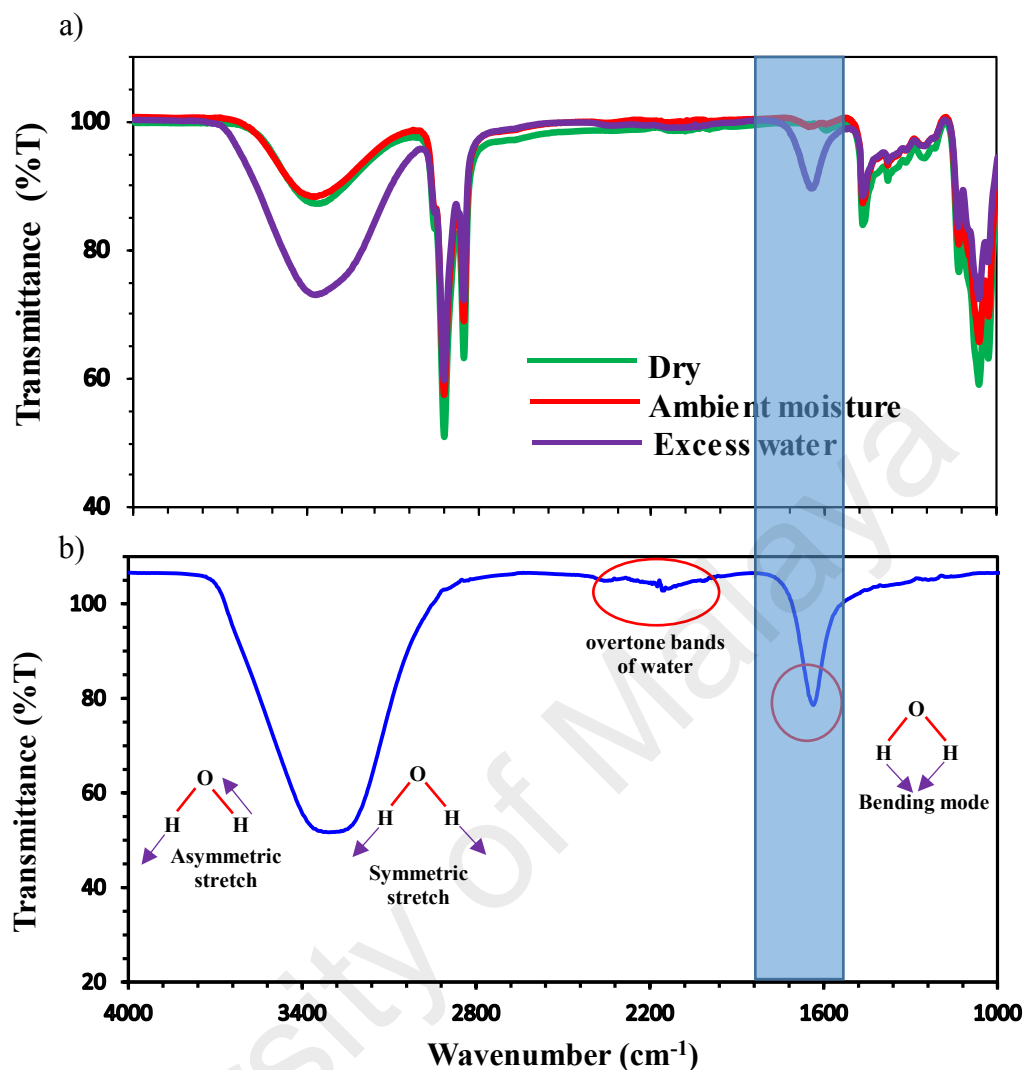


Figure 4.2: (a) FTIR spectra for α -Man-OC₁₄C₁₀ at the room temperature in dry (after lyophilized in freeze dryer for at least 48 h), left in ambient moisture for 96 h and in excess water form and (b) FTIR spectra for water at room temperature.

Differential Scanning Calorimeter (DSC)

The phase transition temperatures for the samples were obtained calorimetrically during the DSC second heating cycles to remove the thermal history and minimize the kinetic effect. The enthalpy change (ΔH) associated with the phase transition was determined by integrating the endothermic peaks and the baseline in Figure 4.3. Typical peaks for a liquid crystal phase transition consisting of melting and clearing phase transition peaks are clearly seen for the longer chain members.

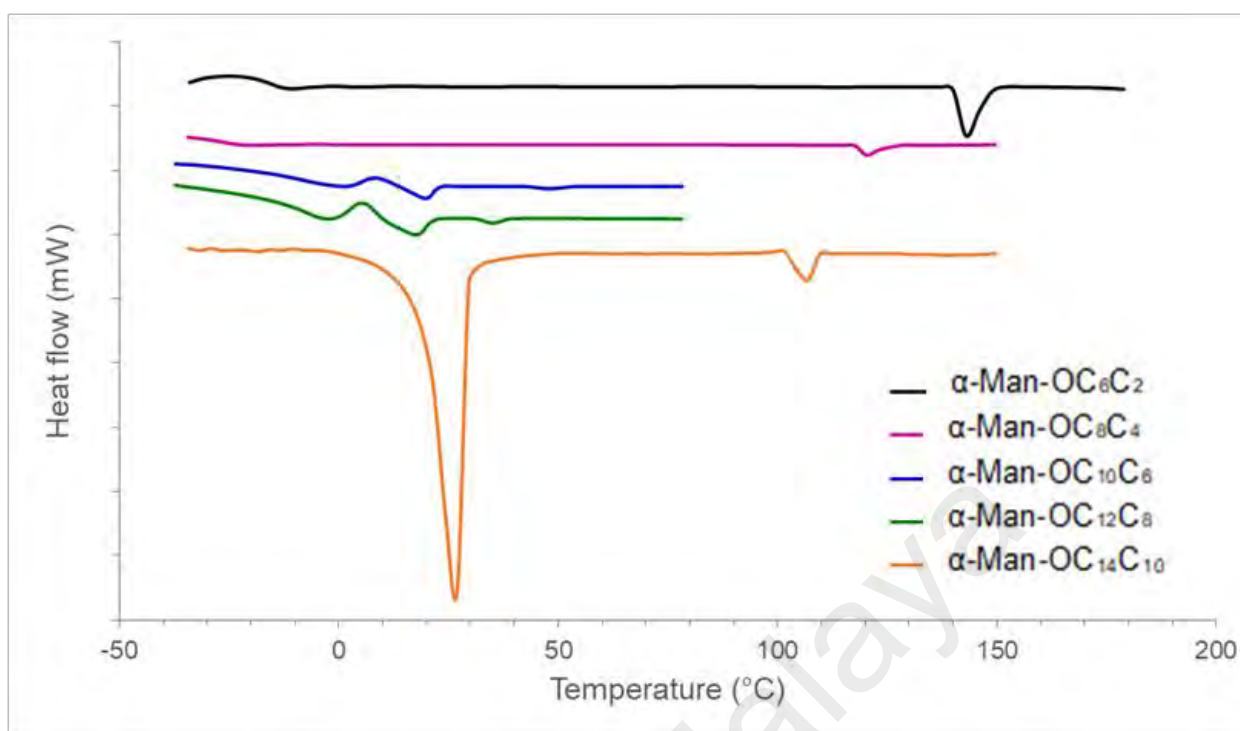


Figure 4.3: DSC thermograms for dry α -D-mannosides at a heating scanning rate of $5^{\circ}\text{C min}^{-1}$.

While the shorter chain counterparts exhibited only isotropic phase transition. In addition, the thermograms of α -Man-OC₆C₂, α -Man-OC₈C₄, α -Man-OC₁₀C₆ and α -Man-OC₁₂C₈ also give a step-like shaped peak which corresponds to the glass transitions was detected below 0°C . A glass transition is an endothermic event, a change in heat capacity that is depicted by a shift in the baseline. It is considered the softening point of the material or the melting of the amorphous regions of a semi-crystalline material. Below the glass transition, i.e. at a lower temperature, the phase structure is a glassy liquid crystalline which best described as a frozen version of the liquid crystal. Due to the presence of a glass transition, it is possible that a liquid crystalline melting transition possesses too low enthalpy to be detected in the performed scans (Sagnella, 2011).

However, such a transition was not apparent in α -Man-OC₁₄C₁₀. For these Guerbet chain mannosides, there is no apparent trend in this glass transition, partly because glass transition is a kinetic phenomenon and path dependent. Ogawa reported there is no effect

of T_G upon the increasing of the chain length for monoalkylated glucosides (Ogawa et al., 2013).

Table 4.1: Thermotropic phase transition temperatures T_m (melting) and T_C (clearing) for the dry α -D-mannosides determined by DSC and OPM. Asterisk (*) indicates the value is determined by OPM. ΔH_m and ΔH_C are enthalpies associated with melting and clearing transitions respectively. Errors in the measured transition temperature $\pm 1^\circ\text{C}$, while error in the enthalpy change is $\pm 0.1 \text{ kJ mol}^{-1}$. The symbol “-” denotes unknown value due to the limitation of the calorimeter. Phase identification is by OPM, except for the glassy phase, is which identified as lamellar glass ($L_{\alpha G}$). For comparison monoalkylated mannosides and other Guerbet α -glycosides (glucose, galactose and xylose) are included.

Lipid	Phase	$T_G/^\circ\text{C}$	$T_m/^\circ\text{C}$	ΔH_m (kJ mol ⁻¹)	Phase	$T_C/^\circ\text{C}$	ΔH_C (kJ mol ⁻¹)	Phase
α -Man-OC ₆ C ₂	$L_{\alpha G}$	-13	-		L_α	143 145*	2.5	L_2
α -Man-OC ₈ C ₄	$L_{\alpha G}$	-25	-		L_α	120 120*	1.3	L_2
α -Man-OC ₁₀ C ₆	$L_{\alpha G}$	-1	20	2.2	L_α	48 51*	0.3	L_2
α -Man-OC ₁₂ C ₈	$L_{\alpha G}$	-2	17	3.0	V_2	35 40*	0.3	L_2
α -Man-OC ₁₄ C ₁₀	Cr	-	26	10.0	H_2	106 108*	0.5	L_2
Monoalkylated mannosides' melting and clearing transition temperatures from OPM (Vill et al., 1989)								
α -Man-OC ₈	Cr	-	55		L_α	134		L_1
α -Man-OC ₁₀	Cr	-	65		L_α	153		L_1
α -Man-OC ₁₂	Cr	-	74		L_α	162		L_1
Different branched chain glycolipids' melting and clearing transition temperatures from OPM in references (Hashim et al., 2011; Rodzi, 2006), while † indicates data from (Zahid et al., 2013)								
α -Glc-OC ₆ C ₂	Cr	-	-		L_α	105		L_2
α -Glc-OC ₁₀ C ₆	Cr	-	-		L_α	48 †		L_2
α -Glc-OC ₁₄ C ₁₀	Cr	-	-		H_2	118		L_2
α -Gal-OC ₆ C ₂	Cr	-	-		L_α	67		L_2
α -Gal-OC ₈ C ₄	Cr	-	-		L_α, V_2	43, 50		L_2
α -Gal-OC ₁₀ C ₆	Cr	-	-		V_2	51 †		L_2
α -Gal-OC ₁₂ C ₈	Cr	-	-		H_2	80		L_2
α -Gal-OC ₁₄ C ₁₀	Cr	-	-		H_2	104		L_2

Table 4.1 shows the measured ΔH values of the phase transition temperature for α -D-mannosides and their corresponding enthalpy obtained from the DSC thermograms. In general, both melting and clearing transitions of α -D-mannosides were represented by a broader peak, which is characteristic of a not so cooperative process (Wunderlich et al., 1997). This indicates the transformation to the fluid phase may involve a region with two

co-existing phases implying a weak first order transition (Atkins & Atkins, 1992). Under these circumstances, heat capacity no longer shows a distinct narrow peak at a given temperature; instead, a melting/clearing process takes place over a range of temperature (Wunderlich et al., 1997).

Optical Polarizing Microscopy (OPM)

The mesomorphic behaviour of dry lipid as a function of the temperature was further studied by OPM to identify the phases of these systems using the texture identification technique. Generally, anisotropic phases such as lamellar and hexagonal are visible under polarized light with distinctly different birefringent textures, where the latter gives much larger domains compared to the former. On the contrary, the cubic and micellar phases are optically isotropic and black when observed under crossed polarizers since the light passing through the sample is refracted in every direction. These isotropic samples (i.e. cubic and micellar) can be distinguished from each other because when pressed the former is more viscous than the latter (Liew et al., 2015). The clearing transition temperatures of the pure compounds obtained from OPM are tabulated in Table 4.1.

The shortest chain compound, α -Man-OC₆C₂ transformed from liquid crystal to an isotropic phase at 143°C with $\Delta H = 2.5 \text{ kJ mol}^{-1}$ as observed from the DSC thermogram (see Figure 4.3). Figure 4.4(a) shows the OPM of α -Man-OC₆C₂ texture obtained at the room temperature. On heating, the dry α -Man-OC₆C₂ became isotropic completely at 145°C. In the cleared state, the sample was fluid, suggesting the phase to be an inverse micellar (L₂) phase. When the sample was cooled, birefringent texture started to develop at 143°C, which was consistent with a lamellar (L_a) phase. No further changes were observed upon cooling the material to the room temperature (Figure 4.4(a)). The DSC thermogram of α -Man-OC₈C₄ showed that the sample undergo isotropization at 120°C and the enthalpy change of first order was calculated as $\Delta H = 1.3 \text{ kJ mol}^{-1}$. Upon heating

under optical polarizing microscope, the sample cleared at 120°C and on cooling, a focal conic texture with stronger birefringence than α -Man-OC₆C₂ appeared below 113°C and remained at the room temperature (Figure 4.4(b)). No other phase transitions were observed on DSC thermograms upon subsequent heating and cooling for α -Man-OC₆C₂ and α -Man-OC₈C₄. This implies the solid to liquid crystal phase transition (melting point) occurred at a much lower temperature beyond the range of the lowest experimental temperature (−40°C). In addition, this suggests that these two compounds are already liquid crystalline at room temperature.

On the other hand, the middle chain compound, α -Man-OC₁₀C₆ gave a melting transition from the crystal phase at 20°C, and the associated enthalpy change was 2.2 kJ mol^{−1}. Upon further heating, the transition into isotropic state gave a clearing temperature at 48°C ($\Delta H = 0.3$ kJ mol^{−1}). The neat compound of α -Man-OC₁₀C₆ became clear at 51°C when observed under optical polarizing microscope. On cooling, an oily-streak pattern like texture was produced until it reached room temperature (Figure 4.4(c)) which could be attributed as the lamellar structure. Similarly, α -Man-OC₁₂C₈ melted at 17°C with $\Delta H = 3.0$ kJ mol^{−1}. At 35°C, α -Man-OC₁₂C₈ changed from liquid crystalline state to the isotropic liquid state with $\Delta H = 0.3$ kJ mol^{−1}. No birefringence was observed for α -Man-OC₁₂C₈ upon heating or cooling (Figure 4.4(d)), and the compound appeared to be a viscous isotropic sample at 40°C, suggesting that α -Man-OC₁₂C₈ adopted a cubic phase before transforming to an isotropic liquid. Its space group identity shall be confirmed by the small angle x-ray scattering experiment. Meanwhile, α -Man-OC₁₄C₁₀ melted from the crystal phase at 26°C ($\Delta H = 10.0$ kJ mol^{−1}). At 106°C, α -Man-OC₁₄C₁₀ undergo isotropization and the enthalpy change was calculated as $\Delta H = 0.5$ kJ mol^{−1}. In the case of dry α -Man-OC₁₄C₁₀, the sample exhibited birefringence upon heating, but completely changed to an isotropic phase at 108°C. When the sample is cooled to room

temperature from its isotropic state, it produced the typical fan shape-like texture (Figure 4.4(e)) of an inverse hexagonal (H_2) phase.

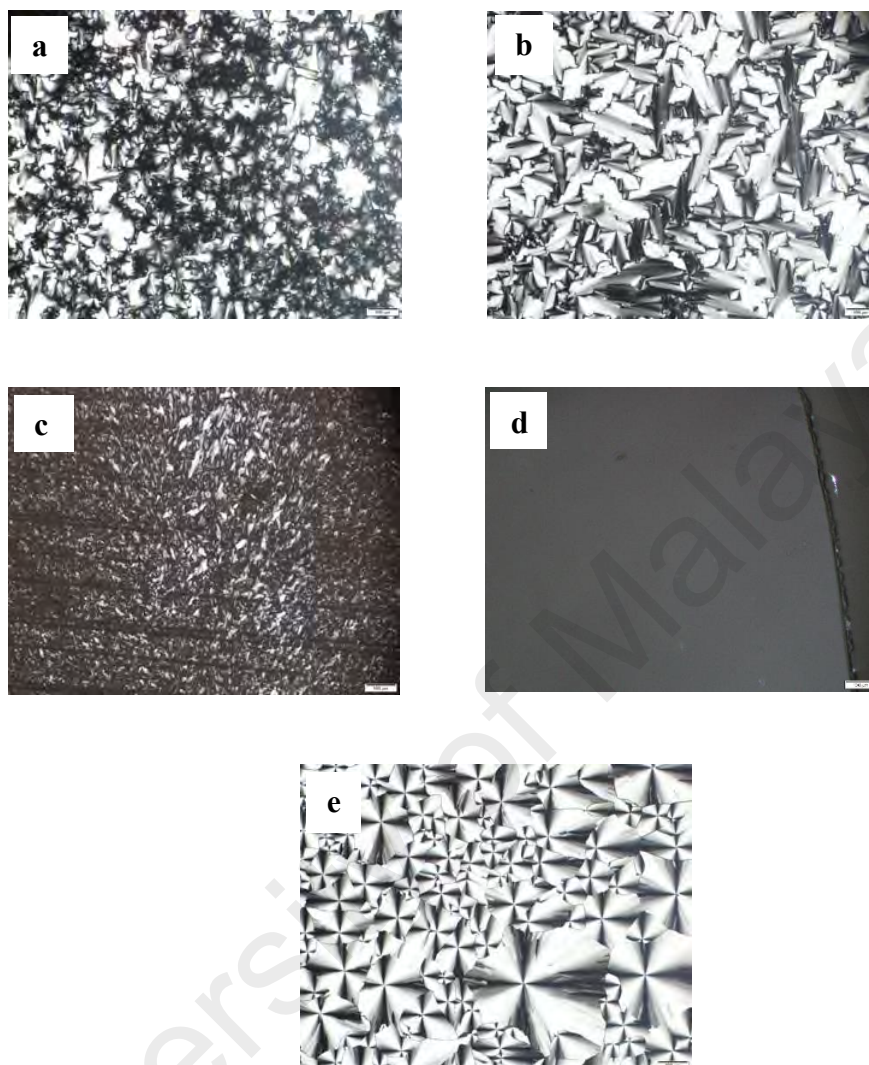


Figure 4.4: Textures of dry α -D-mannosides at 25°C, viewed under an optical polarizing microscope with x10 magnification: (a-c) show textures of L_α phase observed for α -Man-OC₆C₂, α -Man-OC₈C₄ and α -Man-OC₁₀C₆ respectively; (d) a cubic phase V₂ is observed for α -Man-OC₁₂C₈; (e) H_2 for α -Man-OC₁₄C₁₀.

The enthalpy values of melting transition for α -Man-OC₁₄C₁₀ is significantly larger than that of α -Man-OC₁₀C₆ and α -Man-OC₁₂C₈ of a liquid crystalline to isotropic state transition (clearing transition), indicating that these compounds had undergone a transition directly from a highly ordered crystalline phase to the less ordered liquid crystalline phase (Liew et al., 2015). Additionally, the results show that the clearing points of all samples obtained by OPM confirmed the clearing points determined by DSC. The

slight variation in the clearing temperature between the DSC and OPM is attributed to the different rate of decomposition in aluminum pan and glass slide respectively.

In general, the introduction of chain branching decreases the clearing and melting temperatures, yielding liquid crystallinity at ambient. A similar effect was observed for other compounds, for example galactosides and glucosides when a double bond is introduced (Mannock & McElhaney, 2004; Vill et al., 2000). Table 4.1 shows a clear decrease of melting temperatures, T_m for branched-chain α -D-mannosides with respect to their straight analogues due to the increased conformational disorder in the hydrophobic region created by the chain branching. Another notable difference between the dialkylated mannoside to its monoalkylated counterpart is the clearing point, T_c in which the latter increased with the chain length of the hydrophobic region. This is expected since by chain elongation more energy is required to break interactions to form the isotropic phase. The trend is consistent until the molecular weight ratio of the sugar head to that of tail groups is in the balance. After reaching the balance point, a further increase in the chain length will lower the clearing temperature due to increased motion of the hydrocarbon chains.

Such behaviour was not observed for branched-chain α -D-mannosides series as has been the case for other Guerbet glycolipids with glucose (Hashim et al., 2011) and galactose (Hashim et al., 2006) head groups. However, the two shorter chained Guerbet mannosides (α -anomer) have higher clearing temperatures than those of the other monosaccharide sugars which are epimerically related (see Table 4.1). The mannoside with a mannose sugar has an axial OH group at C-2. Compared to corresponding glucoside which has 2-OH in the equatorial position, the mannoside volume decreases and hence increase the clearing points. This axial OH group effect give largest volume reduction at C-4 position which lead to the isotropization of galactoside occurred at much lower temperature than that of mannoside (Vill et al., 1989). This observation is supported by computational work on α -anomer of octyl- gluco, galacto and mannosides using a

density functional theory with the application of atoms in molecules (AIM) analysis (Ahmadi et al., 2017; Mosapour Kotena et al., 2014). It was shown that the mannose head forms an additional hydrogen bond of type HO3...O2 between OH on C-3 and oxygen (O2) on C-2 on mannose ring. The glucose head forms an additional hydrogen bond of type HO4...O6 between OH on C-4 and oxygen (O6) of the hydroxymethyl on glucose ring. The galactose head forms an additional hydrogen bond of type HO4...O3 between OH on C-4 and oxygen (O3) on C-3 on galactose ring. However, no general trend in T_c can be formed for this collection of Guerbet glycosides, since these also have special anomeric (α/β) relationship (Ahmadi et al., 2017; Mosapour Kotena et al., 2014).

Unlike anhydrous single chain mannosides where only L_α is observed, the double chain mannosides exhibit various liquid crystal phases. The homologous chain behaviour of Guerbet glycosides is also interesting, since apart from showing the usual tendency expected for the straight-chain series, the longer chain length seems to promote thermotropic inverse curved phases (V_2 and H_2) (Liew et al., 2015) as seen by the OPM textures (see Figure 4.4).

Small Angle X-ray Scattering (SAXS)

SAXS experiments were performed to elucidate the mesophase identity and to show well-defined Bragg peaks, from which the size of the unit cell in the crystalline structure can be obtained. Figure 4.5 shows a 1-D SAXS pattern of anhydrous Guerbet branched α -D-mannosides at 25°C. The scattering pattern of α -Man-OC₆C₂ showed a sharp scattering signal in the low q -region (0.305 \AA^{-1}) indicating a typical L_α phase with a d -spacing of 20.6 \AA (see Figure 4.5(a)). The higher-order peaks were not observable and it is common to observe only a few scattering peaks from liquid crystalline phases due to liquid-like short range positional order.

The SAXS pattern of α -Man-OC₈C₄ is expected to give characteristic peaks of a L _{α} phase as determined by OPM. Nevertheless, the compound showed a sequence of scattering peaks that could be associated with the coexistence of two lamellar phases at 25°C (see Figure 4.5(b)). This was inferred by the appearance of two pairs of Bragg peaks, each pair in the positional ratio 1:2. We assumed the first and fourth peaks to be related with d-spacing of 22.6 Å whereas the second and fifth peaks can be associated with d-spacing of 19.5 Å. The third (middle) peak could not be assigned to any specific lattice and speculate this phase is metastable on cooling and the compound may take a long time to equilibrate to its original phase. This metastable phase which is dependent on temperature and other variables, can exist over long time so that no spontaneous conversion to the ground state occurs in a reasonable time frame. The lack of reversibility in lipid phase transitions which is shown by the occurrence of distinct metastable phases that replace the equilibrium ones in cooling scans has been observed in phospholipid and glycolipid dispersion (Tenchov, 1991). Figure 4.6(b) shows the SAXS pattern of α -Man-OC₈C₄ at different temperatures. The same reflection was obtained at 37°C. However, with increasing temperature to 50°C, this metastable phase starts to merge into a lamellar phase with d-spacing of 22.4 Å. This implies that the sample has reached to its equilibrium state. All the five peaks at 25°C and 37°C merge into a single peak on further heating up to 90°C. At 120°C, a broad diffuse spectrum was observed indicating an isotropic liquid.

Dry α -Man-OC₁₀C₆ is expected to give characteristic peaks of L _{α} phase as previously determined by OPM. However, its SAXS pattern shows uncommon characteristic peaks at 25°C which are different from the lamellar reflection order (see Figure 4.5(c)). The scattering pattern contains ten sharp lines below 0.6 Å⁻¹ (see Figure 4.6(c) at 25°C). By this SAXS pattern, the phase for α -Man-OC₁₀C₆ remains unclear even after an overnight cooling to the room temperature from its isotropic phase. The unassignable SAXS pattern may indicate a possible involvement of kinetic retardations

during the phase transformations of α -Man-OC₁₀C₆. This non equilibrium behavior may be related to a slow rearrangement mode and requires a longer time for the system to return to equilibrium (Elouatib et al., 1991; Fouret et al., 1991; Tenchov, 1991). When the temperature is increased to 37°C, this metastable phase starts to merge into a lamellar phase with d -spacing of 23.8 Å (Figure 4.6(c)). The d -spacing value remains the same at 50°C.

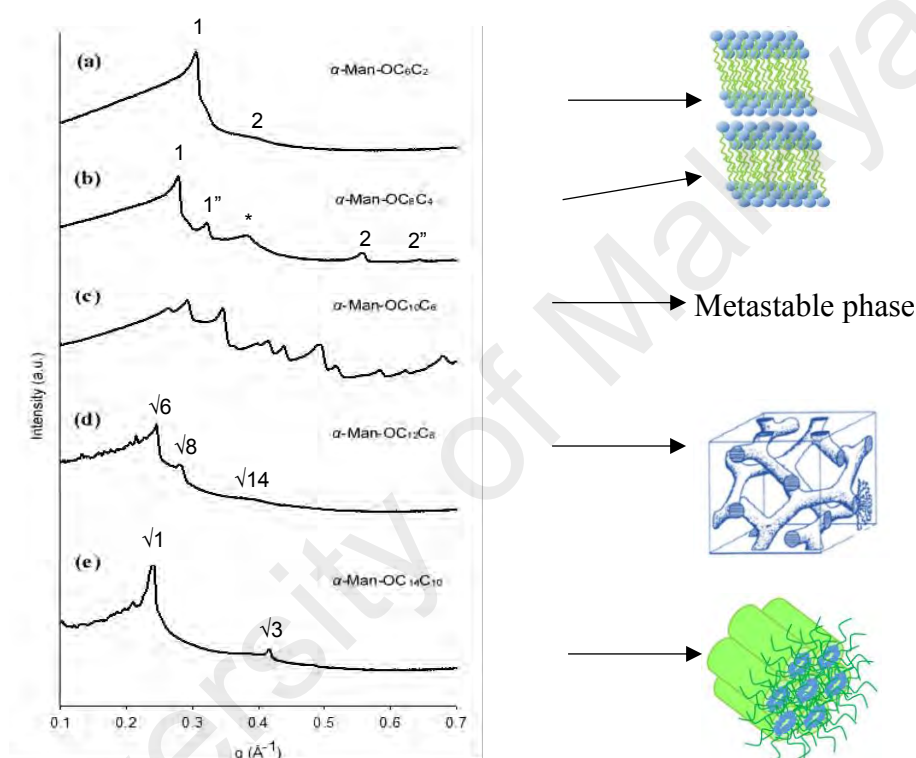


Figure 4.5: Small angle X-ray scattering patterns from dry Guerbet branched α -D-mannosides at 25°C. Patterns are offset along the y-axis for clarity. (a) L_α ; (b) the two different size L_α phases and *unassigned peak; (c) a metastable phase; (d) an inverse bicontinuous cubic phase with space group $Ia3d$ phase and (e) H_2 phase.

A typical scattering of $Ia3d$ space group with Bragg peaks corresponding to the reflection $\sqrt{6}$, $\sqrt{8}$, $\sqrt{14}$ were observed for α -Man-OC₁₂C₈ at 25°C as shown in Figure 4.5(d). Often, for a bicontinuous cubic gyroid G-mesophase ($Ia3d$) only the first three peaks are strong enough to be observed. The calculated lattice parameter is 63.0 Å. Since this is a dry thermotropic system, the microstructure of an inverse bicontinuous cubic phase has a three-dimensional (3-D) periodic structure comprising of a single, continuous

bilayer that divides the hydrophilic region into two interpenetrating but nonconnecting nanosize channels, draped over a triply periodic minimal surface (TPMS) (Sagnella et al., 2009; Seddon & Templer, 1995; Zahid et al., 2013).

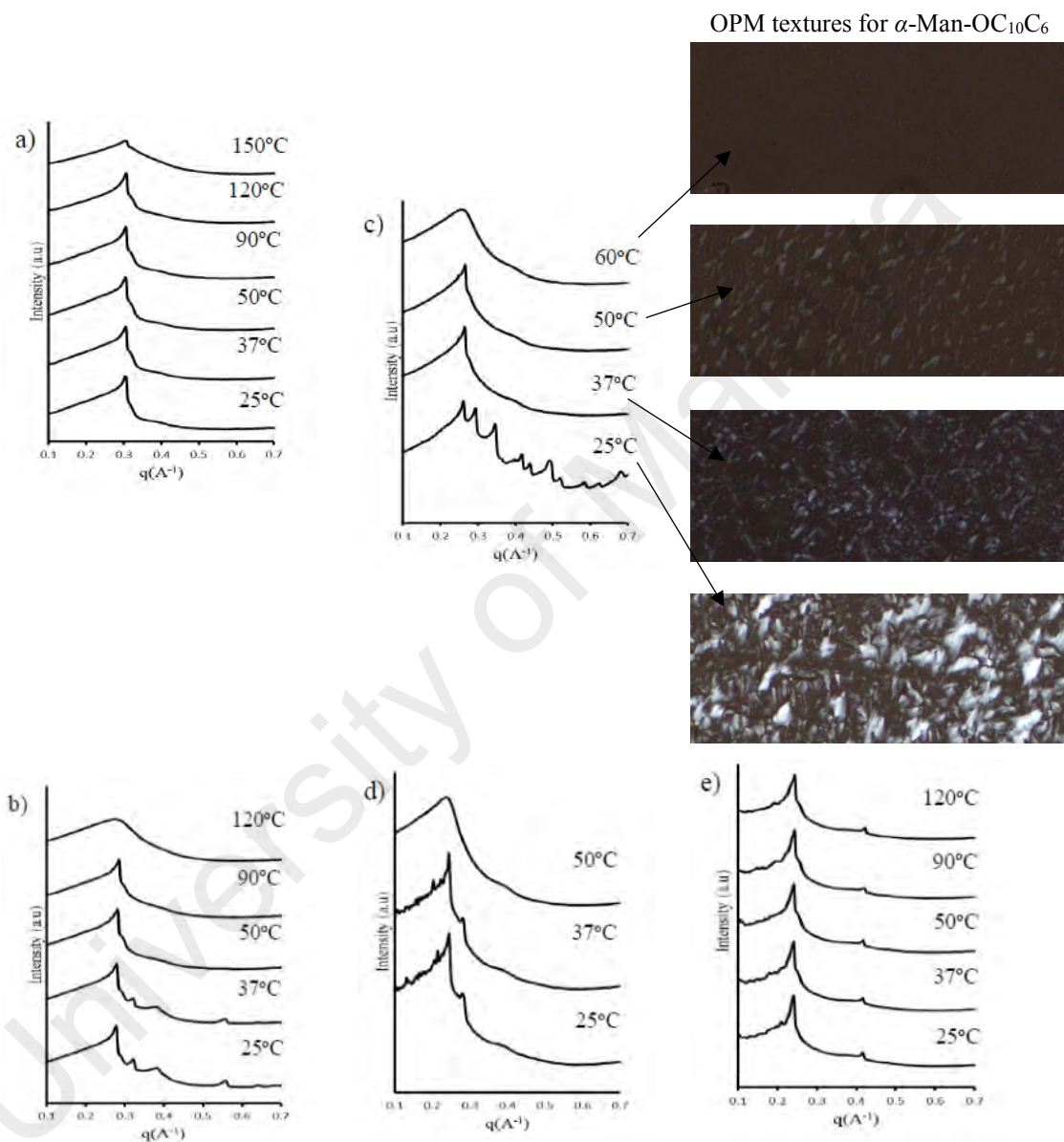


Figure 4.6: SAXS pattern as a function of temperature for (a) α -Man-OC₆C₂, (b) α -Man-OC₈C₄, (c) α -Man-OC₁₀C₆, (d) α -Man-OC₁₂C₈ and (e) α -Man-OC₁₄C₁₀.

The SAXS pattern for dry α -Man-OC₁₄C₁₀ is shown in Figure 4.5(e). The compound has the typical scattering pattern for a H₂ phase which are the first order peak, and a significantly weak $\sqrt{3}$ peak giving lattice parameter of 30.0 Å at 25°C. This result

confirms the assignment for corresponding OPM texture. All SAXS data for the dry α -D-mannosides at 25°C is tabulated in Table 4.2.

Table 4.2: Small angle X-ray scattering data of the dry α -D-mannosides at 25°C. Error in lattice parameter measurements is ± 0.1 Å. * indicates measurements taken at 37°C.

Lipid	Phase	Lattice parameter (Å)
α -Man-OC ₆ C ₂	L _{α}	20.6
α -Man-OC ₈ C ₄	L _{α} ^a	19.5 and 22.6
α -Man-OC ₁₀ C ₆	metastable L _{α} ^b	- *23.8 Å
α -Man-OC ₁₂ C ₈	V ₂ (<i>Ia3d</i>)	63.0 Å
α -Man-OC ₁₄ C ₁₀	H ₂	30.0 Å

^aTwo lamellar phases of different size. ^bL _{α} phase is obtained at 37°C.

Typical wide angle X-ray scattering patterns of α -Man-OC₈C₄ and α -Man-OC₁₀C₆ in Figure 4.7 show a diffuse peak located at 1.35 Å⁻¹ (correspond to a spacing of 4.7 Å) which arises from the liquid-like disorder of the alkyl chain within the bilayer.

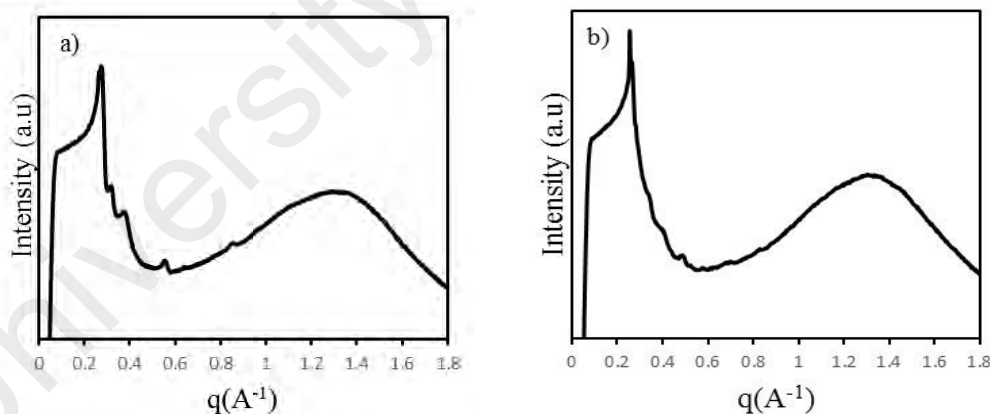


Figure 4.7: WAXS pattern at 25°C for (a) α -Man-OC₈C₄ and (b) α -Man-OC₁₀C₆.

4.2.2 Lyotropic phase behaviour

Depending on the chain length, branched chain α -D-mannosides in dry state may give rise to non-lamellar phases as previously reported for the corresponding glycolipids having xylose and glucose headgroups (Brooks et al., 2011; Liew et al., 2015). When

these systems are hydrated, more curve phases are expected to be observed. Water penetration scan which involves the direct observation via cross-polarized optical microscope of the lyotropic phases was employed to access the lyotropic phase behaviour of the α -D-mannosides (see Figure 4.8). Generally, anisotropic phases such as lamellar and hexagonal phases are visible under polarized light with distinctly different birefringent textures, where the latter gives much larger domains compared to the former. On the contrary, the cubic and micellar phases were optically isotropic and black when observed under crossed polarizers and could be distinguished from each other because the former was more viscous when pressed than the latter.

The observed phase for α -Man-OC₆C₂ is provided in Figure 4.8(a). Upon addition of water at 30°C, the water rich side of the sample turned to an isotropic phase, presumably a normal micelle (L₁) replacing the L _{α} phase. In Figure 4.8(b), the dry α -Man-OC₈C₄ compound initially gave strong birefringence with L _{α} texture under OPM at room temperature. Water contact penetration experiments for this compound gave a single phase where the L _{α} phase remained at the water-rich side of the phase and gave a focal conic texture. On the other hand, the water penetration scan for α -Man-OC₁₀C₆ (see Figure 4.8(c)) shows the formation of a viscous isotropic phase at higher water content, replacing the birefringence texture by neat α -Man-OC₁₀C₆. The longer branched alkyl chain α -Man-OC₁₂C₈ and α -Man-OC₁₄C₁₀ displayed an inverse hexagonal phase in the contact penetration method as shown in Figure 4.8(d) and 4.8(e), respectively. These phases will be further confirmed by using the small angle X-ray scattering.

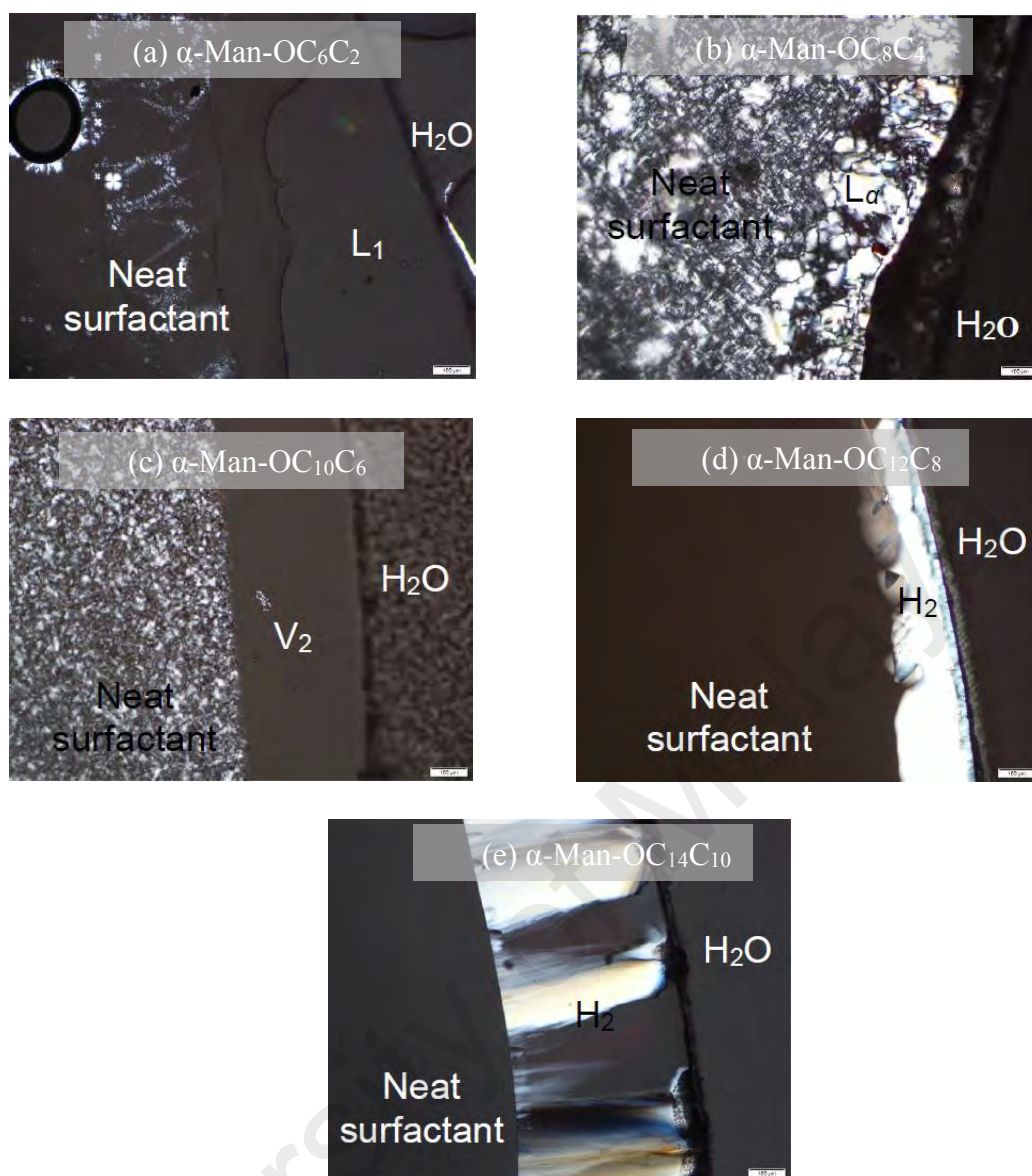


Figure 4.8: Contact penetration textures of Guerbet branched α -D-mannosides, viewed under an optical polarizing microscope (x10) at 30°C after 60 min: (a) normal micellar, L_1 ; (b) lamellar, L_α ; (c) inverse cubic, V_2 ; (d) inverse hexagonal, H_2 and (e) inverse hexagonal, H_2 .

The Guerbet branched-chain mannoside compounds were studied under excess water at 25°C and prepared at 90% (w/w) water concentration. At this concentration, a two-phase region between water and a liquid-like medium or liquid-crystal phase were detected which indicates that an excess water point has been achieved.

At full hydration, no sharp scattering peak was observed for the shortest compound i.e. α -Man-OC₆C₂, consistent with it being completely soluble in excess water, forming

an L_1 micellar solution (see Figure 4.9(a)). Its SAXS pattern gives a broad peak centered at q of ca. 0.27 \AA^{-1} , with a lattice parameter or cell–cell distance of 24.6 \AA .

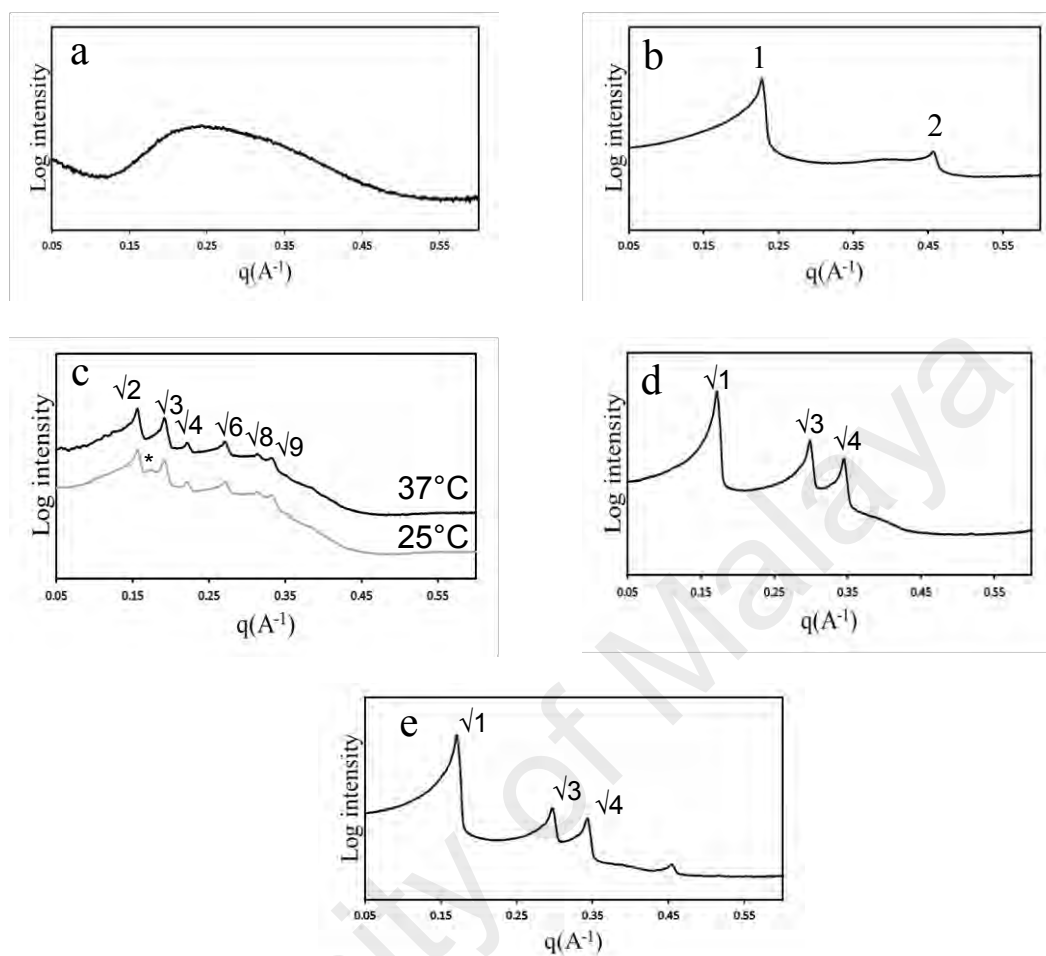


Figure 4.9: SAXS patterns for Guerbet branched-chain mannoside in excess water at 25°C . (a) L_1 micellar solution; (b) lamellar, L_α ; (c) inverse bicontinuous cubic ($Pn3m$) and asterisk, * indicates an extra peak of another phase present at 25°C and the peak merged into a $Pn3m$ at 37°C . (d) inverse hexagonal, H_2 and (e) inverse hexagonal, H_2 .

While the dry $\alpha\text{-Man-OC}_8\text{C}_4$ showed a scattering peaks that could be associated with coexistence of two lamellar phase at 25°C , in excess water it shows an L_α structure with d-spacing of 27.2 \AA (see Figure 4.9(b)). In an excess water condition, $\alpha\text{-Man-OC}_{10}\text{C}_6$ undergoes a solvation process to form an inverse bicontinuous cubic phase, V_2 . As can be seen from Figure 4.9(c), the Bragg peaks are observed with spacing ratios of $\sqrt{2}, \sqrt{3}, \sqrt{4}, \sqrt{6}, \sqrt{8},$ and $\sqrt{9}$ which are the first six allowed reflections of space group $Pn3m$ with a lattice parameter of 56.5 \AA . However, at 25°C , there is a trace amount of another phase present, possibly resulting from local drying. When the temperature is increased to 37°C ,

the peak merged into a $Pn3m$ cubic phase and their lattice parameter are equal to within the error. The presence of the small peak is probably due to local drying and not chemical degradation since Guerbet glycosides are expected to be stable within the temperature range studied (Zahid et al., 2013).

Both fully hydrated α -Man-OC₁₂C₈ and α -Man-OC₁₄C₁₀ were found to give an inverse hexagonal H₂ phase with strong characteristic peaks of $\sqrt{1}$, $\sqrt{3}$, and $\sqrt{4}$ (see Figure 4.9(d) and 4.9(e)). The lattice parameter for both longer chain members were 41.9 Å and 42.2 Å. The assignment of inverse phase behaviour is based upon the very low solubility of the lipids and the presence of the cubic or hexagonal phases against the excess water interface thereby suggesting stability against dilution (Tiddy, 1980). The lattice parameters for the self-assembly structures in excess water are reported in Table 4.3.

Table 4.3: Small-angle X-ray scattering data of the fully hydrated α -D-mannosides at 25°C. Error in lattice parameter is ± 0.1 Å.

Lipid	Phase	Lattice parameter (Å)
α -Man-OC ₆ C ₂	L ₁	24.6
α -Man-OC ₈ C ₄	L _{α}	27.2
α -Man-OC ₁₀ C ₆	V ₂ ($Pn3m$)	56.5
α -Man-OC ₁₂ C ₈	H ₂	41.9
α -Man-OC ₁₄ C ₁₀	H ₂	42.2

All lyotropic phases formed by the α -D-mannoside homologous series are related to the average interfacial mean curvature due to the difference of the lateral pressure of the head group region and the hydrocarbon chain region. A zero curvature is formed when the pressure of the head group region is similar to the pressure of the hydrocarbon chain region, the monolayer of the lipids will be flat i.e. lamellar. A positive curvature monolayer (normal phase) will be obtained when pressure of head group is larger than the pressure of the hydrocarbon chain region. Meanwhile, a negative curvature will form when pressure of head group region is lower (inverse phase). Among the five solvated compounds, the lateral pressure in the head group remains the same while hydrocarbon

parts depends on the alkyl chain length. The shortest chain compound α -Man-OC₆C₂ has positive mean curvature i.e. the lateral pressure of head group is greater than the hydrocarbon chain region which resulted in formation of L₁ micellar solution. As for α -Man-OC₈C₄, the mean curvature is zero indicating its lateral pressure in both head group and hydrocarbon parts is balanced. The longer chain compounds i.e. α -Man-OC₁₀C₆, α -Man-OC₁₂C₈ and α -Man-OC₁₄C₁₀ which formed the inverse bicontinuous (V₂) and hexagonal (H₂) phases indicate they have large pressure in the hydrocarbon chain and this causes the mean curvature to be negative. The pressure in the hydrocarbon chain region is expected to be larger for lipids with longer chains i.e. α -Man-OC₁₄C₁₀ followed by α -Man-OC₁₂C₈ and α -Man-OC₁₀C₆.

CHAPTER 5: CONCLUSION

The study of Guerbet glycolipids often involves controlled and designed synthesis from which trends of their properties are elucidated. The aim of this work was to synthesize and characterize Guerbet branched chained glycolipids by using mannose sugar as the head group. Herein, five branched-chain synthetic glycolipids namely α -Man-OC₆C₂, α -Man-OC₈C₄, α -Man-OC₁₀C₆, α -Man-OC₁₂C₈ and α -Man-OC₁₄C₁₀ with different total alkyl chain length from C₈ to C₂₄ carbons have been synthesized. The anomeric purity of these compounds was confirmed to be at least 98% using two different techniques, namely NMR and TLC. The syntheses required three steps which are peracetylation, glycosidation and deacetylation. The chemical structure of the compounds was confirmed by NMR spectroscopy to identify the anomeric purity of the compounds.

The effect of chain branching on their thermotropic liquid crystalline phases were investigated by OPM, DSC and SAXS. DSC results showed unique phase transition patterns including glass transitions for these series of compounds. The glass transition temperature (T_g) characterizes the temperature below which frozen lamellar glassy phase exists. It is always lower than the melting temperature (T_m) of the crystalline state of the material. A comparison of the five compounds with different chain length shows different glassy behavior, where α -Man-OC₆C₂, α -Man-OC₈C₄, α -Man-OC₁₀C₆ and α -Man-OC₁₂C₈ give step-like shaped peaks detected below 0°C but no such transition is apparent in α -Man-OC₁₄C₁₀. In addition, a comparison of the five compounds also showed that they have different phases as the chain length increases. The shortest chain α -Man-OC₆C₂ was found to exhibit L_α phase in dry and micellar, L_1 by addition of excess water. Meanwhile, α -Man-OC₈C₄ gave a focal conic texture with a strong birefringence suggesting that this too was a lamellar phase in both dry and excess water conditions which has been confirmed with the SAXS studies. The dry sample of α -Man-OC₁₀C₆ gave

strong birefringence under OPM at room temperature especially at the sample edge and suggesting a lamellar phase during this transition. However, it shows a metastable phase during the measurement of SAXS and $Pn3m$ phase upon on the water penetration study. The dry sample of a α -Man-OC₁₂C₈ gives an inverse bicontinuous cubic phase (V_2) but gave an inverse hexagonal H_2 upon the addition of water. In addition, α -Man-OC₁₄C₁₀ exhibit H_2 phase in both dry and excess of water content.

In order to understand the structure property behaviour of these mannosides, we compared their phase behaviour with other branched chain glycolipids, namely those with glucose and galactose headgroups, since mannose, glucose and galactose are epimerically related. α -D-mannosides is only slightly different from α -D-glucosides at the C2 position where the hydroxyl group axial in the case of mannose and equatorial for glucose. This small difference resulted in a greater intralayer hydrogen bond within the sugar headgroup region for the former. This difference is reflected in the clearing transition of mannosides which are higher than the glucosides at the short chain. However, there was no change on the phase behavior of α -Man-OC₁₀C₆ and α -Glc-OC₁₀C₆ and both give L_α . There is a slight difference on the longest chain compounds where α -Glc-OC₁₄C₁₀ has a high clearing temperature than α -Man-OC₁₄C₁₀ even though both give H_2 phase.

When comparing with the α -D-mannosides and α -D-galactosides as a head group, the clearing transition of mannosides were higher than the galactoside except for the second highest chain (see Table 3.1). One example from the list of compounds studied, α -Man-OC₁₂C₈ was expected to give H_2 phase since the tail are increasing but instead it gives V_2 phase while α -Gal-OC₁₂C₈ gives a H_2 phase. The shortest chain for both compounds give L_α phase as expected. It shown that the change in head group (i.e mannosides, glucosides and galactosides) seem important in controlling the liquid crystal behaviour.

We can conclude that the behaviour of these compounds depend to the chain lengths and the effects of the parameters like temperature and the added solvent. This study has successfully accomplished the main objectives of the thesis which are to synthesize a series of glycolipids namely α -D-mannopyranoside with different branched alkyl chain lengths and the study of their behaviour on thermotropic and lyotropic studied as well as for their nanostructural parameter. There are several works that can be proposed on future research where we can further it by study their surfactant properties like the critical micelle concentration (CMC), bound water by deuterium NMR as well as for the application towards biomedicine like drug delivery and cosmetics.

University of Malaysia

References

- Ahmadi, S., ManickamAchari, V., Hussain, Z., & Hashim, R. (2017). Epimeric and anomeric relationship of octyl- α -D-gluco/galactosides: Insight from density functional theory and atom in molecules studies. *Computational and Theoretical Chemistry*, *1108*, 93–102.
- Alexandridis, P., Olsson, U., & Lindman, B. (1998). A record nine different phases (four cubic, two hexagonal, and one lamellar lyotropic liquid crystalline and two micellar solutions) in a ternary isothermal system of an amphiphilic block copolymer and selective solvents (water and oil). *Langmuir*, *14*(10), 2627–2638.
- An, J. G., Hina, S., Yang, Y., Xue, M., & Liu, Y. (2016). Characterization of liquid crystals: A literature review. *Reviews on Advanced Materials Science*, *44*(4), 398–406.
- Atkins, P.W. (1992). *The elements of physical chemistry*. United Kingdom: Oxford University Press Oxford.
- Auroux, A. (2013). *Calorimetry and thermal methods in catalysis*. New York: Springer Series in Material Science.
- Baron, M. (2001). Definitions of basic terms relating to low-molar-mass and polymer liquid crystals (IUPAC Recommendations 2001). *Pure and Applied Chemistry*, *73*(5), 845–895.
- Boons, G.J. (1996). Recent developments in chemical oligosaccharide synthesis. *Contemporary Organic Synthesis*, *3*(3), 173–200.
- Brooks, N. J., Hamid, H. A., Hashim, R., Heidelberg, T., Seddon, J. M., Conn, C. E., & Hussen, R. S. D. (2011). Thermotropic and lyotropic liquid crystalline phases of Guerbet branched chain-D-glucosides. *Liquid Crystals*, *38*(11–12), 1725–1734.
- Brown, G. (2012). *Liquid crystals and biological structures*. New York: Elsevier.
- Brown, M.F. (2012). Curvature forces in membrane lipid–protein interactions. *Biochemistry*, *51*(49), 9782–9795.
- Carlton, R.A. (2011). *Pharmaceutical microscopy*. New York: Springer.
- Chen, Y., Ma, P., & Gui, S. (2014). Cubic and hexagonal liquid crystals as drug delivery systems. *BioMed Research International*, *2014*, S1–S12.
- Chen, J.H., & Lubensky, T. (1976). Landau-Ginzburg mean-field theory for the nematic to smectic-C and nematic to smectic-A phase transitions. *Physical Review A*, *14*(3), 1202(1–6).
- Chung, T.S. (1986). The recent developments of thermotropic liquid crystalline polymers. *Polymer Engineering & Science*, *26*(13), 901–919.
- Collings, P.J. (2002). *Liquid crystals: Nature's delicate phase of matter*. New Jersey: Princeton University Press.

- Collings, P.J., & Hird, M. (1997). *Introduction to liquid crystals: Chemistry and physics*. London: CRC Press.
- Daley, R.F., & Daley, S.J. (2017, December). *Organic Chemistry, 2005*. Retrieved from: <http://www.ochem4free.info/node/1>.
- Darbeau, R.W. (2006). Nuclear magnetic resonance (NMR) spectroscopy: A review and a look at its use as a probative tool in deamination chemistry. *Applied Spectroscopy Reviews*, 41(4), 401–425.
- Davis, B.G. (2000). Recent developments in oligosaccharide synthesis. *Journal of the Chemical Society, Perkin Transactions 1*, 14, 2137–2160.
- Daw, J. (2008). *Measurement of specific heat capacity using differential scanning calorimeter*, in report of US department of energy national laboratory. Unites States: Idaho National Laboratory.
- Deamer, D. W., Leonard, R., Tardieu, A., & Branton, D. (1970). Lamellar and hexagonal lipid phases visualized by freeze-etching. *Biochimica et Biophysica Acta (BBA)-Biomembranes-Review on Biomembranes*, 219(1), 47–60.
- Dellinger, T.M., & Braun, P.V. (2004). Lyotropic liquid crystals as nanoreactors for nanoparticle synthesis. *Chemistry of Materials*, 16(11), 2201–2207.
- Demetzos, C. (2008). Differential scanning calorimetry (DSC): A tool to study the thermal behavior of lipid bilayers and liposomal stability. *Journal of Liposome Research*, 18(3), 159–173.
- Dierking, I. (2003). *Textures of liquid crystals*. Weinheim: Wiley-VCH.
- Dimensional metrology for nanofabrication. (2017, December). Retrieved from <https://www.nist.gov/programs-projects/dimensional-metrology-nanofabrication>.
- Elouatib, A., Gors, C., & Fouret, R. (1991). Metastable phases in kinetics of phase transformations in the frozen liquid crystal 4-ethoxybenzylidene-4'-n-butylaniline. *Liquid Crystals*, 9(4), 539–550.
- Emwas, A.H.M. (2015). The strengths and weaknesses of NMR spectroscopy and mass spectrometry with particular focus on metabolomics research, in *metabonomics. Method in Molecular Biology*, 1277, 161–193.
- Ewing, D. F., Goodby, J. W., Haley, J. A., Kelly, S. M., Letellier, P., & Mackenzie, G. (1997). N-Acyl-beta-D-glycopyranosylamines and 2-alkylamido-2-deoxy-alpha/beta-D-glucopyranoses: Relationship between molecular structure and mesomorphism. *Liquid Crystals*, 23(5), 759–769.
- Fontell, K. (1990). Cubic phases in surfactant and surfactant-like lipid systems. *Colloid and Polymer Science*, 268(3), 264–285.

- Fontell, K., Fox, K.K., & Hansson, E. (1985). On the structure of the cubic phase II in some lipid-water systems. *Molecular Crystals and Liquid Crystals Letters*, 1(1–2), 9–17.
- Forrest, B.J., & Reeves, L. W. (1981). New lyotropic liquid crystals composed of finite nonspherical micelles. *Chemical Reviews*, 81(1), 1–14.
- Fouret, R., Elouatib, A., Gors, C., More, M., Pepy, G., & Rosta, L. (1991). Metastable phases and kinetics of phase transformations in quenched liquid crystals: Phase transitions. *A Multinational Journal*, 33(1–4), 209–225.
- FP82HT Thermal Microscopy Hot Stage. (2017, October). Retrieved from <http://www.totalss.co.kr/?c=product/MettlerToledo&cat=Melting+point+Values&uid=176>.
- Fu, Y., Jeong, S. H., & Park, K. (2006). Preparation of fast dissolving tablets based on mannose. *Polymeric Drug Delivery II*, 23, 340–351.
- Garegg, P. J., Konradsson, P., Kvarnstrom, I., Norberg, T., Svensson, S. C. T., & Wigilius, B. (1985). Studies on Koenigs-Knorr glycosidations. *Acta Chemica Scandinavica B*, 39(7), 569–577.
- Garidel, P., Kaconis, Y., Heinbockel, L., Wulf, M., Gerber, S., Munk, A., & Brandenburg, K. (2015). Self-organisation, thermotropic and lyotropic properties of glycolipids related to their biological implications. *The Open Biochemistry Journal*, 9, 49–72.
- Goodby, J. W., Gortz, V., Cowling, S. J., Mackenzie, G., Martin, P., Plusquellec, D., & Chambert, S. (2007). Thermotropic liquid crystalline glycolipids. *Chemical Society Reviews*, 36(12), 1971–2032.
- Gray, G.W. (1987). *Thermotropic liquid crystals*. New York: John Wiley & Sons Inc.
- Guo, C., Wang, J., Cao, F., Lee, R.J., & Zhai, G. (2010). Lyotropic liquid crystal systems in drug delivery. *Drug Discovery Today*, 15(23), 1032–1040.
- Hashim, R., Mirzadeh, S. M., Heidelberg, T., Minamikawa, H., Yoshiaki, T., & Sugimura, A. (2011). A reevaluation of the epimeric and anomeric relationship of glucosides and galactosides in thermotropic liquid crystal self-assemblies. *Carbohydrate Research*, 346(18), 2948–2956.
- Hashim, R., Hashim, H. H. A., Rodzi, N. Z. M., Hussien, R. S. D., & Heidelberg, T. (2006). Branched chain glycosides: Enhanced diversity for phase behavior of easily accessible synthetic glycolipids. *Thin Solid Films*, 509(1), 27–35.
- Hashim, R., Sugimura, A., Minamikawa, H., & Heidelberg, T. (2012). Nature-like synthetic alkyl branched-chain glycolipids: A review on chemical structure and self-assembly properties. *Liquid Crystals*, 39(1), 1–17.
- Hato, M., & Minamikawa, H. (1996). The effects of oligosaccharide stereochemistry on the physical properties of aqueous synthetic glycolipids. *Langmuir*, 12(6), 1658–1665.

- Ho, M. W., Haffegge, J., Newton, R., Zhou, Y. M., Bolton, J. S., & Ross, S. (1996). Organisms as polyphasic liquid crystals. *Bioelectrochemistry and Bioenergetics*, 41(1), 81–91.
- Hu, X., Shi, Y., Zhang, P., Miao, M., Zhang, T., & Jiang, B. (2016). D-Mannose: Properties, production, and applications: An overview. *Comprehensive Reviews in Food Science and Food Safety*, 15(4), 773–785.
- Hyde, S.T. (2001). Identification of lyotropic liquid crystalline mesophases. *Handbook of applied surface and colloid chemistry*. New York: John Wiley & Sons Inc.
- Jacques, D.A., & Trehwella, J. (2010). Small-angle scattering for structural biology expanding the frontier while avoiding the pitfalls. *Protein Science*, 19(4), 642–657.
- Jenkins, J.T. (1978). Flows of nematic liquid crystals. *Annual Review of Fluid Mechanics*, 10(1), 197–219.
- Jin, J.I. (1980). Thermotropic liquid crystalline polyesters with rigid or flexible spacer groups. *British Polymer Journal*, 12(4), 132–146.
- Johansson, E. (2015). *Design and synthesis of multivalent sialoside inhibitors of adenoviruses and enteroviruses against infections of human ocular cells*. (Degree's thesis). UMEA University, Sweden.
- Kaasgaard, T., & Drummond, C.J. (2006). Ordered 2-D and 3-D nanostructured amphiphile self-assembly materials stable in excess solvent. *Physical Chemistry Chemical Physics*, 8(43), 4957-4975.
- Kawamoto, H. (2002). The history of liquid-crystal displays. *Proceedings of the IEEE*, 90(4), 460–500.
- Kelker, H. (1973). History of liquid crystals. *Molecular Crystals and Liquid Crystals*, 21(1–2), 1–48.
- Kelker, H. (1988). Survey of the early history of liquid crystals. *Molecular Crystals and Liquid Crystals*, 165(1), 1–43.
- Kikhney, A.G., & Svergun, D.I. (2015). A practical guide to small angle X-ray scattering (SAXS) of flexible and intrinsically disordered proteins. *FEBS Letters*, 589(19), 2570–2577.
- Killian, J.A. & Kruijff, B.D. (2004). Nonbilayer lipids affect peripheral and integral membrane proteins via changes in the lateral pressure profile. *Biochimica et Biophysica Acta (BBA)-Biomembranes*, 1666(1), 275–288.
- Kishikawa, K., Inoue, T., Sasaki, Y., Aikyo, S., Takahashi, M., & Kohmoto, S. (2011). Generation of biaxiality in smectic A phases by introduction of intermolecular perfluoroarene–arene and C–H/F interactions, and the non-odd–even effect of the molecules in their transition temperatures and layer distances. *Soft Matter*, 7(16), 7532–7538.

- Kleman, M., & Lavrentovich, O. (2009). Liquids with conics. *Liquid Crystals*, 36 (10–11), 1085–1099.
- Knothe, G. (2002). Synthesis, applications, and characterization of Guerbet compounds and their derivatives. *Lipid Technology*, 14, 101–104.
- Koeltzow, D.E., & Urefer, A.D. (1984). Preparation and properties of pure alkyl glucosides, maltosides and maltotriosides. *Journal of the American Oil Chemists Society*, 61(10), 1651–1655.
- Kozlowski, J.T. & Davis, R.J. (2013). Heterogeneous catalysts for the Guerbet coupling of alcohols. *ACS Catalysis*, 3(7), 1588–1600.
- Ladeveze, S., Laville, E., Despres, J., Mosoni, P., & Potocki-Veronese, G. (2017). Mannoside recognition and degradation by bacteria. *Biological Reviews*, 92(4), 1969–1990.
- Lagerwall, J.P. & Scalia, G. (2012). A new era for liquid crystal research: Applications of liquid crystals in soft matter nano-, bio-and microtechnology. *Current Applied Physics*, 12(6), 1387–1412.
- Lauger, J., Linemann, R., & Richtering, W. (1995). Shear orientation of a lamellar lyotropic liquid crystal. *Rheologica Acta*, 34(2), 132–136.
- Liao, G., Zewe, S. K., Hagerty, J., Hashim, R., Abeygunaratne, S., Vill, V., & Jakli, A. (2006). Thermotropic liquid crystalline properties of amphiphilic branched chain glycolipids. *Liquid Crystals*, 33(3), 361–366.
- Liew, C. Y., Salim, M., Zahid, N. I., & Hashim, R. (2015). Biomass derived xylose Guerbet surfactants: Thermotropic and lyotropic properties from small-angle X-ray scattering. *RSC Advances*, 5(120), 99125–99132.
- Loewenstein, A. & Igner, D. (1991). Deuterium NMR studies of n-octyl α and β -glucopyranoside liquid-crystalline systems. *Liquid Crystals*, 10(4), 457–466.
- Maibaum, L., Dinner, A.R., & Chandler, D. (2004). Micelle formation and the hydrophobic effect. *The Journal of Physical Chemistry B*, 108(21), 6778–6781.
- Makowski, L. (2010). Characterization of proteins with wide-angle X-ray solution scattering (WAXS). *Journal of Structural and Functional Genomics*, 11(1), 9–19.
- Mannock, D.A., & McElhaney, R.N. (2004). Thermotropic and lyotropic phase properties of glycolipid diastereomers: Role of headgroup and interfacial interactions in determining phase behaviour. *Current Opinion in Colloid & Interface Science*, 8(6), 426–447.
- Matsushita, T., & Koseki, S. (2005). Theoretical study on mesogenic core structures of nematic liquid crystalline compounds. *The Journal of Physical Chemistry B*, 109(28), 13493–13498.

- Mazzobre, M.A.F., Aguilera, J.M., & Buera, M.A.P. (2003). Microscopy and calorimetry as complementary techniques to analyze sugar crystallization from amorphous systems. *Carbohydrate Research*, 338(6), 541–548.
- Messinger, H., Aulmann, W., Kleber, M., & Koehl, W. (2007). Investigations on the effects of alkyl polyglucosides on development and fertility. *Food and Chemical Toxicology*, 45(8), 1375–1382.
- Mettler Toledo Fp90 Central Processor For The Fp900 Thermosystem. (2017, October). Retrieved from: <http://www.terapeak.com/worth/mettler-toledo-fp90-central-processor-for-the-fp900-thermosystem/291774403920/>.
- Microscopy primer. (2017, December). Retrieved from: <http://www.olympuslifescience.com/en/microscoperesource/primer/techniques/polarized/desenarmontcompensator/>.
- Mosapour Kotena, Z., Behjatmanesh-Ardakani, R., & Hashim, R. (2014). AIM and NBO analyses on hydrogen bonds formation in sugar-based surfactants (α/β -D-mannose and n-octyl- α/β -D-mannopyranoside): A density functional theory study. *Liquid Crystals*, 41(6), 784–792.
- Movasaghi, Z., Rehman, S., & Rehman, D.I. (2008). Fourier transform infrared (FTIR) spectroscopy of biological tissues. *Applied Spectroscopy Reviews*, 43(2), 134–179.
- Murphy, D.B., *Fundamentals of light microscopy and electronic imaging*. 2002, Canada: John Wiley & Sons.
- Nanda, R. & Damodaran, K. (2018). A review of NMR methods used in the study of the structure and dynamics of ionic liquids. *Magnetic Resonance in Chemistry*, 56(2), 62–72.
- Neto, A.M.F., & Salinas, S.R. (2005). *The physics of lyotropic liquid crystals: Phase transitions and structural properties*. Unites States: OUP Oxford.
- Nguan, H., Ahmadi, S., & Hashim, R. (2014). Molecular dynamics simulations of the lyotropic reverse hexagonal (H_{II}) of guerbet branched-chain β -D-glucoside. *Physical Chemistry Chemical Physics*, 16(1), 324–334.
- Nilsson, F., Soderman, O., & Johansson, I. (1996). Physical-chemical properties of the n-octyl β -D-glucoside/water system. A phase diagram, self-diffusion NMR, and SAXS study. *Langmuir*, 12(4), 902–908.
- O'Lenick Jr, A. J. (2001). Guerbet chemistry. *Journal of Surfactants and Detergents*, 4(3), 311–315.
- Ogawa, S., Asakura, K., & Osanai, S. (2013). Thermotropic and glass transition behaviors of n-alkyl β -D-glucosides. *RSC Advances*, 3(44), 21439–21446.
- Pacwa-Plociniczak, M., Płaza, G. A., Piotrowska-Seget, Z., & Cameotra, S. S. (2011). Environmental applications of biosurfactants: Recent advances. *International Journal of Molecular Sciences*, 12(1), 633–654.

- Parshin, A.M. (2013). Domain structures in nematic liquid crystals on a polycarbonate surface. *International Journal of Molecular Sciences*, 14(8), 16303–16320.
- Pauw, B.R. (2017, December). *How to do a perfect saxs measurement*. Retrieved from: http://www.lookingatnothing.com/wp-content/uploads/2011/04/imp_userguide.pdf.
- Polakova, M., Belanova, M., Petrus, L., & Mikusova, K. (2010). Synthesis of alkyl and cycloalkyl α -D-mannopyranosides and derivatives thereof and their evaluation in the mycobacterial mannosyltransferase assay. *Carbohydrate Research*, 345, 1339–1347.
- Pope, C.G. (1997). X-ray diffraction and the bragg equation. *Journal of Chemical Education*, 74(1), 129.
- Prost, J. (1995). *The physics of liquid crystals*. Britain: Oxford University Press.
- Qi, H., & Hegmann, T. (2006). Formation of periodic stripe patterns in nematic liquid crystals doped with functionalized gold nanoparticles. *Journal of Materials Chemistry*, 16(43), 4197–4205.
- Rager, T., Meyer, W.H., & Wegner, G. (1999). Micelle formation of poly (acrylic acid)-block-poly (methyl methacrylate) block copolymers in mixtures of water with organic solvents. *Macromolecular Chemistry and Physics*, 200(7), 1672–1680.
- Rajabalaya, R., et al.(2017). Oral and transdermal drug delivery systems: Role of lipid-based lyotropic liquid crystals. *Drug Design, Development and Therapy*, 11, 393(1–14).
- Rather, M.Y., & Mishra, S. (2013). β -Glycosidases: An alternative enzyme based method for synthesis of alkyl-glycosides. *Sustainable Chemical Processes*, 1(1), 7(1–15).
- Rizvi, T.Z. (2003). Liquid crystalline biopolymers: A new arena for liquid crystal research. *Journal of Molecular Liquids*, 106(1), 43–53.
- Rodríguez, C., & Kunieda, H. (2000). Effect of electrolytes on discontinuous cubic phases. *Langmuir*, 16(22), 8263–8269.
- Rodzi, N. (2006). *Branched chain galactosides and melibiosides: synthesis and mesomorphic properties*. (Master's thesis). University of Malaya, Kuala Lumpur.
- Rojas, O.J. (2016). *Cellulose chemistry and properties: Fibers, nanocelluloses and advanced materials*. New York: Springer.
- Sagnella, S. M., Conn, C. E., Krodkiewska, I., & Drummond, C. J. (2009). Soft ordered mesoporous materials from nonionic isoprenoid-type monoethanolamide amphiphiles self-assembled in water. *Soft Matter*, 5(23), 4823–4834.
- Sagnella, S.M. (2011). Anandamide and analogous endocannabinoids: a lipid self-assembly study. *Soft Matter*, 7(11), 5319–5328.
- Sasaki, D. (2008). *Glycolipids: New research*. New York: Nova Publishers.

- Savage, P.B., Teyton, L., & Bendelac, A. (2006). Glycolipids for natural killer T cells. *Chemical Society Reviews*, 35(9), 771–779.
- Schmidt, R.R., & Kinzy, W. (1994). Change of the anomeric hydroxylgroup by bromine or chlorine as the first step. *Advances in Carbohydrate Chemistry and Biochemistry*, 50, 21–123.
- Schmidt, R.R. (1986). New methods for the synthesis of glycosides and oligosaccharides are there alternatives to the koenigs-knorr method. *Angewandte Chemie International Edition in English*, 25(3), 212–235.
- Schmid, K., & Tesmann, H. (2001). *Alkyl polyglycosides*. Unites States of America: Sufactant Science Series.
- Schnablegger, H., & Singh, Y. (2011). *The SAXS guide: Getting acquainted with the principles*. Austria: Anton Paar.
- Seddon, J., & Templer, R. (1995). Polymorphism of lipid-water systems. *Handbook of Biological Physics*, 1, 97–160.
- Seddon, J.M. (1990). Structure of the inverted hexagonal (H_{II}) phase, and non-lamellar phase transitions of lipids. *Biochimica et Biophysica Acta (BBA)-Reviews on Biomembranes*, 1031(1), 1–69.
- Shiloach, A., & Blankschtein, D. (1998). Measurement and prediction of ionic/nonionic mixed micelle formation and growth. *Langmuir*, 14(25), 7166–7182.
- Stevenson, C.L., Bennett, D. B., & Lechuga, B.D. (2005). Pharmaceutical liquid crystals: The relevance of partially ordered systems. *Journal of Pharmaceutical Sciences*, 94(9), 1861–1880.
- Szule, J.A., Fuller, N.L., & Rand, R.P. (2002). The effects of acyl chain length and saturation of diacylglycerols and phosphatidylcholines on membrane monolayer curvature. *Biophysical Journal*, 83(2), 977–984.
- Tanbour, R. (2016). Drug delivery systems based on polymeric micelles and ultrasound: A review. *Current Pharmaceutical Design*, 22(19), 2796–2807.
- Tenchov, B. (1991). On the reversibility of the phase transitions in lipid-water systems. *Chemistry and Physics of Lipids*, 57(2-3), 165–177.
- Thomas, W.L. (2008). *Use of Fourier transform infrared (FTIR) spectroscopy to determine the health-promoting index (HPI) of cow's milk*. (Master's thesis). Iowa State University, United States.
- Tiddy, G.J. (1980). Surfactant-water liquid crystal phases. *Physics Reports*, 57(1), 1–46.
- Toshima, K. (2006). Novel glycosylation methods and their application to natural products synthesis. *Carbohydrate Research*, 341(10), 1282–1297.

- Venditti, V., Egner, T.K., & Clore, G.M. (2016). Hybrid approaches to structural characterization of conformational ensembles of complex macromolecular systems combining NMR residual dipolar couplings and solution X-ray scattering. *Chemical Reviews*, 116(11), 6305–6322.
- Vertogen, G., & Wilhelmus, H.D.J. (2012). *Thermotropic liquid crystals, fundamentals*. Berlin: Springer Science & Business Media.
- Vicari, L. (2003). *Optical applications of liquid crystals*. Bristol: Taylor & Francis.
- Vill, V., & Hashim, R. (2002). Carbohydrate liquid crystals: Structure–property relationship of thermotropic and lyotropic glycolipids. *Current Opinion in Colloid & Interface Science*, 7(5), 395–409.
- Vill, V., Bocker, T., Thiem, J., & Fischer, F. (1989). Studies on liquid crystalline glycosides. *Liquid Crystal*, 6, 349–356.
- Vill, V., Von Minden, H. M., Koch, M. H. J., Seydel, U., & Brandenburg, K. (2000). Thermotropic and lyotropic properties of long chain alkyl glycopyranosides: Part I: Monosaccharide headgroups. *Chemistry and Physics of Lipids*, 104(1), 75–91.
- Villandier, N., & Corma, A. (2010). One pot catalytic conversion of cellulose into biodegradable surfactants. *Chemical Communications*, 46(24), 4408–4410.
- Voelker, P.L.M. (2014). Optical methods in rheology: Polarized light imaging. *Chemische Listy*, 108, 697–724.
- Werneck, M.M. (2013). *A guide to fiber bragg grating sensors, in current trends in short- and long period fiber gratings*. Federal University of Rio de Janeiro: Intech.
- Wu, S.T. (1994). *Spatial light modular technology*. New York: Optical Engineering.
- Wunderlich, B., Boller, A., Okazaki, I., Ishikiryama, K., Chen, W., Pyda, M., & Androsch, R. (1999). Temperature-modulated differential scanning calorimetry of reversible and irreversible first-order transitions. *Thermochimica Acta*, 330(1), 21–38.
- Wunderlich, B. (1997). Heat-capacity determination by temperature-modulated DSC and its separation from transition effects. *Thermochimica Acta*, 304, 125–136.
- Yu, B., & Tao, H. (2001). Glycosyl trifluoroacetimidates. Part 1: Preparation and application as new glycosyl donors. *Tetrahedron Letters*, 42(12), 2405–2407.
- Zahid, N.I., Abou-Zied, O.K., & Hashim, R. (2013). Evidence of basic medium in the polar nanochannels of the inverse bicontinuous cubic phase of a Guerbet glycolipid: A steady-state and time-resolved fluorescence study. *The Journal of Physical Chemistry C*, 117(50), 26636–26643.
- Zahid, N. I., Conn, C. E., Brooks, N. J., Ahmad, N., Seddon, J. M., & Hashim, R. (2013). Investigation of the effect of sugar stereochemistry on biologically relevant lyotropic phases from branched-chain synthetic glycolipids by small-angle X-ray scattering. *Langmuir*, 29(51), 15794–15804.

List of Publications and Papers Presented

Publications

Academic Journal

Patrick, M., Zahid, N.I., Kriechbaum, M., & Hashim, R. (2018). Guerbet glycolipids from mannose: Liquid crystals properties. *Liquid Crystals*, 1–7

Salim, M., Wan Iskandar, W. F. N., Patrick, M., Zahid, N. I., & Hashim, R. (2016). Swelling of bicontinuous cubic phases in guerbet glycolipid: Effects of additives. *Langmuir*, 32(22), 5552–5561.

Presentation

1. Preparation and Characterization of Nanostructural Phases of Branched-Chain Glycolipids, 5th International Conference for Young Chemists 2015 (ICYC 2015), 5–7 August 2015, City Bayview Hotel, Georgetown, Pulau Pinang, Malaysia.
2. Amphiphilic Mannosides and Their Liquid Crystal Behaviour. 7th Asian Conference on Colloid and Interface Science (ACCIS2017) , 8–11 August 2017 in Berjaya Times Square Hotel, Kuala Lumpur, Malaysia.

